Design of Luminescent Building Blocks for Supramolecular Triple-helical Lanthanide Complexes†

Claude Piguet,*[a] Jean-Claude G. Bünzli,*[b] Gérald Bernardinelli,[c] Christian G. Bochet[d] and Pascal Froidevaux[b]

[a] *Department of Inorganic, Analytical and Applied Chemistry, University of Geneva, 30 quai E. Ansermet, CH-1211 Geneva 4, Switzerland*

[b] *Institute of Inorganic and Analytical Chemistry, University of Lausanne, BCH, CH-1015 Lausanne, Switzerland*

[c] *Laboratory of X-ray Crystallography, 30 quai E. Ansermet, University of Geneva, CH-1211 Geneva 4, Switzerland*

[d] *Department of Organic Chemistry, University of Geneva, 30 quai E. Ansermet, CH-1211 Geneva 4, Switzerland*

The ligand 2,6-bis(1′-ethyl-5′-methylbenzimidazol-2′-yl)pyridine (L^5) reacts with lanthanide perchlorate in acetonitrile to give the mononuclear triple-helical complexes $[Ln(L^5)_3]^{3+}$ (Ln = Eu, Gd or Tb). The crystal structure of $[Eu(L^5)_3][ClO_4]_3 \cdot 4MeCN$ has been determined, which shows three unco-ordinated perchlorate anions and an $[Eu(L^5)_3]^{3+}$ cation where the three tridentate ligands are wrapped around a pseudo-C_3 axis. The co-ordination sphere around Eu^{III} may be best described as a slightly distorted trigonal-tricapped prism where the six benzimidazole nitrogen atoms occupy the vertices of the prism and the three pyridine nitrogen atoms occupy the capping positions. A detailed geometrical analysis showed that the ethyl groups in L^5 produce a slide of the strands which is responsible for the distortion of the triple-helical structure as exemplified by the low symmetry for the Eu^{III} site in the luminescence spectra of $[Eu(L^5)_3]^{3+}$. Proton NMR spectra in acetonitrile indicate that the triple-helical structure is maintained for $[Ln(L^i)_3]^{3+}$ {Ln = Eu or Tb; L = 2,6-bis(1′-R-benzimidazol-2′-yl)pyridine [R = Me L^1, Et L^2, Pr L^3 or $CH_2C_6H_3(OMe)_2$-3,5 L^4] or L^5} on the NMR time-scale, but the stability of the complexes together with the structural arrangement of the ligands depend on the size of the substituents bound to the benzimidazole nitrogen atoms. Photophysical studies of $[Eu(L^i)_3]^{3+}$ show that these steric effects affect the quantum yield in solution and that methyl groups bound to the 5 positions of the benzimidazole rings in L^5 shift the $\pi \longrightarrow \pi^*$ transitions centred on the ligand, but do not strongly modify the emission properties of $[Eu(L^5)_3]^{3+}$. Extended Hückel calculations give a qualitative insight into the factor controlling the $\pi \longrightarrow \pi^*$ transitions of the ligands and complexes.

The development of stable luminescent lanthanide complexes is a subject of increasing interest mainly due to their potential uses as fluorescent sensors in natural,[1] medical,[2] analytical[3] and bioinorganic[4] sciences, and probes based on Eu^{III} and Tb^{III} are of special interest because of the particularly suitable spectroscopic properties of these ions.[5] To obtain strongly luminescent complexes, the lanthanide metal ion should be bound to chromophoric ligands which are able (*i*) to absorb energy and then transfer it efficiently to the cation and (*ii*) to protect the lanthanide ion from external interactions which usually quench the luminescence.[5,6] Macrocyclic,[7] macrobicyclic[8] or podand-type[9] ligands containing heterocyclic aromatic donor groups have been extensively used for this purpose, but it has been shown recently that much simpler linear oligo-multidentate ligands, such as L^1 or L^8, self-assemble with Ln^{III} to produce stable mono-[10] and di-nuclear[11] triple-stranded helicates which possess well defined and protected metallic sites. In these molecular light-conversion devices the Ln^{III} ions are co-ordinated by nine nitrogen atoms in a pseudo-tricapped trigonal-prismatic arrangement leading to a pseudo-D_3 symmetry for the cations $[Eu(L^1)_3]^{3+}$[10] and $[Eu_2(L^8)_3]^{6+}$[11] as found for the analogous $[Eu(terpy)_3]^{3+}$ (terpy = 2,2′:6′,2″-terpyridyl).[12] Thermodynamic studies[13,14] in acetonitrile have shown that $[Eu(terpy)_3]^{3+}$ exhibits on-off equilibria of the pyridine rings giving predominantly eight-co-ordinate complexes and limiting its use as a luminescent probe in solution since solvent molecules are believed to occupy the free co-ordination sites.[13] To stabilize the mononuclear pseudo-D_3 complexes, Thummel and co-workers[14] introduced ethylene bridges between the pyridine rings (L^7) which preorganize the cisoid conformations required for the complexation to Ln^{III}[10] giving a more stable triple-helical luminescent complex $[Eu(L^7)_3]^{3+}$. However, the difficult preparation[15] of L^7 together with the synthetically tedious modifications and incorporation of terpyridine moieties in oligo-multidentate ligands[16] limit the use of this complex as a building block for extended helical supramolecular structures. Recently, we have developed an alternative approach based on the substitution of the distal pyridine rings of terpy by aromatic benzimidazole rings (L^1) which allows strong intramolecular stacking interactions between the strands and stabilizes the pseudo-D_3 complex $[Ln(L^1)_3]^{3+}$.[10] In contrast to terpyridine moieties, L^1 may easily be derivatized *via* substitution of the benzimidazole nitrogen atoms (L^2–L^4)[10,17] and modification of the central pyridine ring,[18] and L^1 may be incorporated in segmental di-(L^8) and tri-leptic ligands.[11,19] Although crystals and solutions of the 1:1 $[Ln(L^1)(NO_3)_3(MeOH)]$[20] and 1:2 complexes $[Ln(L)_2(NO_3)_2]NO_3$ [L = 2,6-bis(benzimidazol-2′-yl)pyridine][21]

† *Supplementary data available* (No. SUP 57048, 7 pp.): parameters used for EHMO calculations and luminescence spectra. See Instructions for Authors, *J. Chem. Soc., Dalton Trans.*, 1995, Issue 1, pp. xxv–xxx.

Non-SI unit employed: eV ≈ 1.60 × 10^{-19} J.

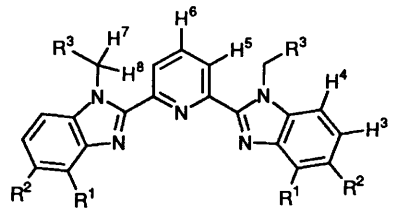

	R^1	R^2	R^3
L^1	H	H	H
L^2	H	H	Me
L^3	H	H	Et
L^4	H	H	$C_6H_3(OMe)_2$-3,5
L^5	H	Me	Me
L^6	Me	H	Me

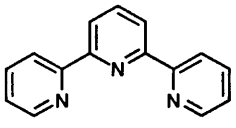

terpy

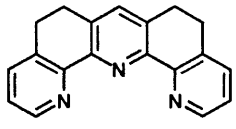

L^7

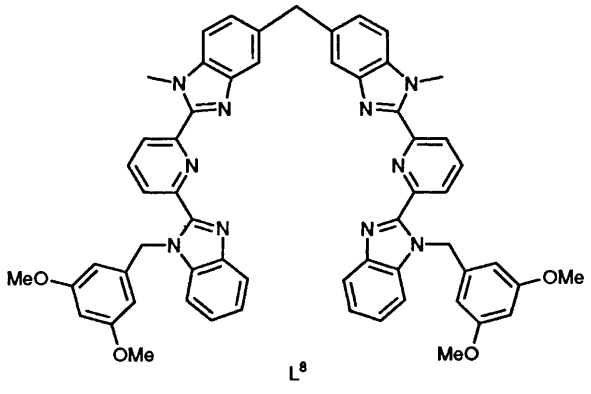

L^8

are strongly luminescent, the triple-helical 1:3 complexes $[Ln(L^1)_3]^{3+}$ (Ln = Eu or Tb) give only weakly luminescent solutions[10] which limit the use of these compounds as molecular light-conversion devices.

In this paper, we report that minor peripheral modifications of the ligand L^1 to give L^2–L^6 significantly influence the structural and photophysical properties of the triple-stranded helical complexes $[Ln(L^i)_3]^{3+}$ (i = 1–5). Data are presented to show that the substitution of the benzimidazole rings with bulky R^3 groups essentially controls the stability and structure of the final complexes while substitution of the six-membered rings in L^5 and L^6 affects the electronic and photophysical properties.

Results and Discussion

Preparation and Properties of the Ligands.—The compounds 2,6-bis(1′-R-benzimidazol-2′-yl)pyridine [R = Me L^1, Et L^2, Pr L^3 or $CH_2C_6H_3(OMe)_2$-3,5 L^4] are obtained according to a previously described two-step strategy based on a double Phillips reaction.[10,17,22] The ligands 2,6-bis(1′-ethyl-X′-methylbenzimidazol-2′-yl)pyridine (X = 5 L^5 or 4 L^6) possess unsymmetrically substituted benzimidazole rings which require a new three-step synthesis based on a recently developed regioselective Phillips reaction (Scheme 1).[19] 4-Chloro-3-nitrotoluene reacts with ethylamine at 130 °C to give compound **1** in satisfactory yield (67%). 3-(*N*-Ethylamino)-2-nitrotoluene **2**

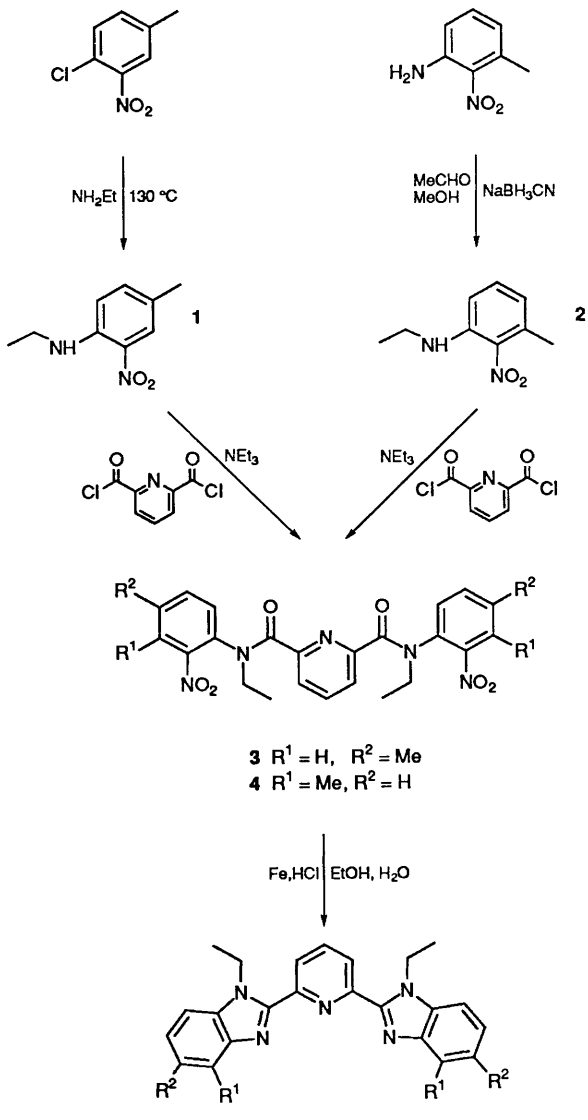

3 R^1 = H, R^2 = Me
4 R^1 = Me, R^2 = H

L^5 R^1 = H, R^2 = Me
L^6 R^1 = Me, R^2 = H

Scheme 1

is prepared by reductive N-alkylation[23] of 3-amino-2-nitrotoluene with acetaldehyde in weakly acidic medium containing $NaBH_3(CN)$.[24] Particular attention has to be paid to keep 3-amino-2-nitrotoluene in large excess during the reaction in order to minimize dialkylation. The reaction of **1** and **2** respectively with 2,6-di(chlorocarbonyl)pyridine under mild conditions give compounds **3** and **4** in 66 and 64% yields. *In-situ* reduction of the nitro groups with metallic iron followed by cyclization under mild conditions (0.2 mol dm^{-3} HCl)[19] converts **3** and **4** into the target ligands L^5 (91%) and L^6 (93%).

In solution, the ligands L^i (i = 1–6) adopt a *trans–trans* conformation[25] and display a broad band in the UV spectra around 31 000 cm^{-1} which is assigned to $\pi \longrightarrow \pi^*$ transitions (Table 1).[17,18,25] For L^i (i = 1–3), where R^3 = alkyl, these transitions lie at 31 150 cm^{-1} and do not significantly depend on R^3. For L^4, the $\pi \longrightarrow \pi^*$ transitions are slightly shifted to lower energies and a shoulder, assigned to internal $\pi \longrightarrow \pi^*$ transitions centred on R^3, is observed at 35 185 cm^{-1}.[18] Compared to L^1 or L^2, the methyl groups bound to the 5 positions of the benzimidazole rings in L^5 shift the $\pi \longrightarrow \pi^*$ transition to lower energies ($\Delta\nu$ = 355 cm^{-1}) while substitution at the 4 positions in L^6 produces a shift to higher energies

Table 1 Electronic spectral data for the ligands L^i (i = 1–6) and the complexes $[Ln(L^i)_3]^{3+}$ (i = 1–5) at 10^{-3} mol dm^{-3} in MeCN[a] and electrochemical reduction potentials in MeCN + 0.1 mol dm^{-3} NBu_4PF_6[b] at 20 °C

Compound	$\pi_2 \longrightarrow \pi^*$	$\pi \longrightarrow \pi^*$	$\pi_1 \longrightarrow \pi^*$	$E_{\frac{1}{2}}$	ΔE_p
L^1		31 150 (32 000)			
		35 710 (17 200) (sh)			
L^2		31 155 (33 000)		−2.02	100
		35 800 (17 800) (sh)			
L^3		31 150 (30 800)			
		35 720 (16 800) (sh)			
L^4		30 980 (31 220)		−1.98	80
		35 185 (21 450) (sh)			
L^5		30 800 (32 800)		−2.03	70
		35 970 (16 155) (sh)			
L^6		31 310 (32 850)		−2.06	100
		36 100 (16 000) (sh)			
$[Eu(L^1)_3]^{3+}$	33 450 (59 400)		27 700 (48 500)		
$[Eu(L^2)_3]^{3+}$	33 180 (57 300)		27 800 (50 100)		
$[Gd(L^2)_3]^{3+}$	33 160 (57 900)		27 655 (51 400)		
$[Tb(L^2)_3]^{3+}$	33 180 (58 000)		27 700 (49 400)		
$[Eu(L^3)_3]^{3+}$	32 360 (56 600)		27 320 (44 300)		
$[Eu(L^4)_3]^{3+}$	35 200 (53 000) (sh)		27 700 (36 000) (sh)		
	31 900 (63 000)				
$[Eu(L^5)_3]^{3+}$	32 070 (49 200)		26 970 (48 500)		
$[Gd(L^5)_3]^{3+}$	32 380 (47 900)		26 880 (47 900)		
$[Tb(L^5)_3]^{3+}$	32 280 (47 900)		26 900 (47 750)		

[a] Energies are given for the maximum of the band envelope in cm^{-1} and ε (in parentheses) in dm^3 mol^{-1} cm^{-1}; sh = shoulder. [b] Electrochemical potentials are given in V *vs.* SCE and $\Delta E_p = E_{pa} - E_{pc}$ in mV. Estimated error on $E_{\frac{1}{2}}$ is ± 0.01 V.

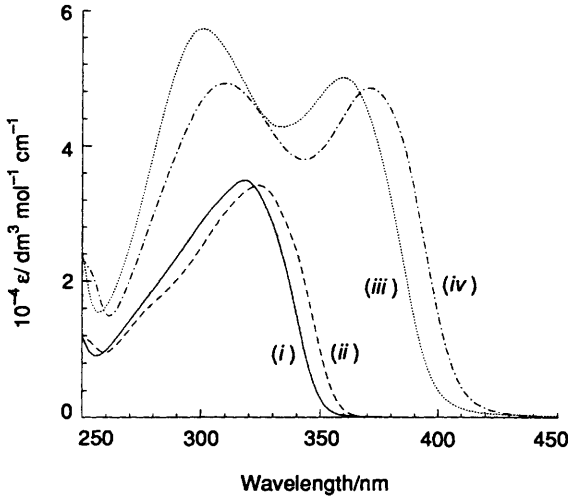

Fig. 1 Electronic spectra of (*i*) L^2, (*ii*) L^5 (dashed line), (*iii*) $[Eu(L^2)_3]^{3+}$ and (*iv*) $[Eu(L^5)_3]^{3+}$ at 10^{-3} mol dm^{-3} in acetonitrile

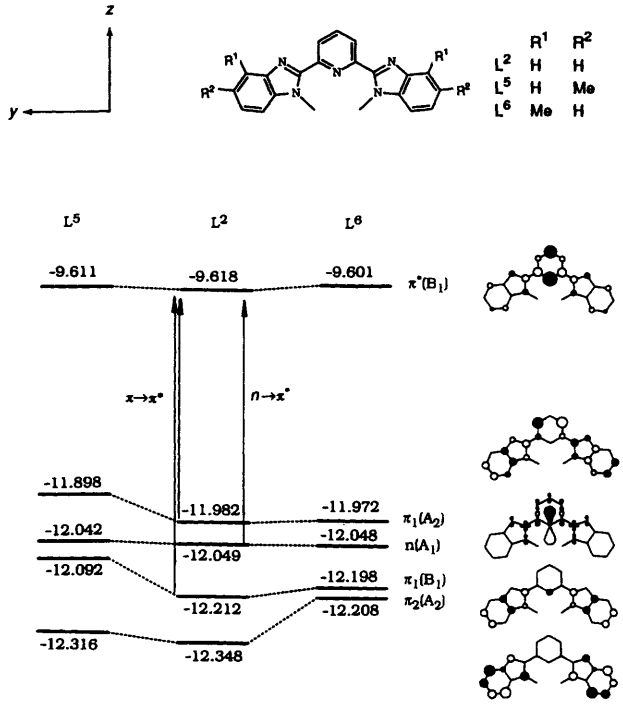

Fig. 2 Schematic representation of frontier orbitals calculated by EHMO[27] for L^2, L^5 and L^6 assuming C_{2v} symmetry. Energies are given in eV and projections of atomic orbital coefficients along the x direction for $\pi^*(B_1)$, $\pi_1(A_2)$, $\pi_1(B_1)$, $\pi_2(A_2)$ and $n(A_1)$ of L^2 are shown on the right

($\Delta\nu$ = 155 cm^{-1}) (Fig. 1, Table 1). As previously reported for L^1 and L^4,[18] we were unable to observe the n $\longrightarrow \pi^*$ transitions for L^i (i = 1–6) which are expected at lower energies.[26] This suggests that the weaker n $\longrightarrow \pi^*$ ($\varepsilon \leqslant 300$ dm^3 mol^{-1} cm^{-1} for terpy in hexane)[26] are masked by the intense $\pi \longrightarrow \pi^*$ transitions for L^i (i = 1–6).

Recently, the extended-Hückel molecular orbital (EHMO) method[27] applied to 2,2′-bipyridine[28] and 4-X-phenylpyridine fragments[18] was shown to give good qualitative agreement with spectroscopic results and we have performed EHMO calculations for L^i (i = 2, 5 or 6) in an attempt to rationalize the UV spectra. The three aromatic rings (two distal benzimidazole rings and one central pyridine ring) were maintained coplanar in transoid conformations assuming C_{2v} symmetry. Bond distances and angles were taken from standard values,[18,29] the methyl groups R^1, R^2 for L^5 and L^6 were fixed in staggered conformations and R^3 was set to H for the calculations (Fig. 2).

The results show that three allowed transitions are expected at low energy for L^2: $n(A_1) \longrightarrow \pi^*(B_1)$ [$n(A_1)$ is essentially the lone pair centred on the pyridine nitrogen atom], $\pi_1(A_2) \longrightarrow \pi^*(B_1)$ and $\pi_1(B_1) \longrightarrow \pi^*(B_1)$ (Fig. 2). For L^6, a $\pi_2(A_2) \longrightarrow \pi^*(B_1)$ transition is expected close to the $\pi_1(B_1) \longrightarrow \pi^*(B_1)$ transition, but no transitions involving other unoccupied levels are expected at low energy for L^i (i = 2, 5 or 6) since the next lowest unoccupied molecular orbital (NLUMO) $\pi^*(A_2)$ lies at significantly higher energies (≈ -9.15 eV). As the $n \longrightarrow \pi^*$ transition is very weak compared to $\pi \longrightarrow \pi^*$,[18,26,30] the $n(A_1) \longrightarrow \pi^*(B_1)$ transition for our qualitative discussion is

neglected. The addition of methyl groups to L^2 to give L^5 leads to a destabilization of both $\pi_1(A_2)$ and $\pi_1(B_1)$ due to interactions with the π orbitals of the methyl[31] while $\pi^*(B_1)$ is almost not affected. This produces a shift of the $\pi \longrightarrow \pi^*$ toward lower energies in agreement with the observed UV spectra when going from L^2 to L^5 (Fig. 1). When the methyl groups are bound to the 4 positions of the benzimidazole rings in L^6, $\pi^*(B_1)$ is slightly more destabilized than $\pi_1(A_2)$ and $\pi_1(B_1)$ leading to a small shift of $\pi \longrightarrow \pi^*$ toward higher energies which is indeed observed in the spectrum of L^6. The weak shoulders observed at high energy for L^i (Table 1) may be tentatively attributed to other $\pi \longrightarrow \pi^*$ transitions since transitions between low-lying π orbitals and $\pi^*(B_1)$ or between π_1 and NLUMO $\pi^*(A_2)$ are expected at higher energies. A detailed analysis of the orbitals found by EHMO analysis leads to the conclusion that methyl groups bound to the benzimidazole six-membered rings in L^5 and L^6 essentially act as π donors[31] and mainly affect the energies of orbitals which possess large $2p_x$ coefficients on the carbon bearing the substituents.

The cyclic voltammograms in MeCN + 0.1 mol dm^{-3} NBu_4PF_6 show the ligands L^2, L^5 and L^6 to be reduced in a single quasi-reversible monoelectronic wave at −2.02, −2.03 and −2.06 V *vs.* saturated calomel electrode (SCE) respectively to give the corresponding radical anions.[18] These values are very close to those found for L^4 (−1.98 V)[18] and terpy (−2.09 V)[32] in very similar conditions. Although the variation of $E_{\frac{1}{2}}$ is small, the observed increasing order $E_{\frac{1}{2}}(L^6) < E_{\frac{1}{2}}(L^5) \leqslant E_{\frac{1}{2}}(L^2)$ confirms the π-acceptor properties of the ligands predicted by EHMO calculations (Fig. 2) since the half-wave potential of the reduction process centred on the ligands reflects the LUMO energy.[33]

Preparation of the Complexes.—The 1:3 complexes $[Ln(L^i)_3][ClO_4]_3$ (i = 2 or 5) are prepared by mixing L^2 or L^5 with stoichiometric amounts of $Ln(ClO_4)_3 \cdot nH_2O$ (n = 6–8) in dichloromethane–acetonitrile. The complexes may be crystallized in good yield by slow diffusion of diethyl ether into an acetonitrile solution to give X-ray quality prisms (white for Ln = Gd or Tb and yellow for Ln = Eu). Four solvent molecules have been found in the crystal structure of $[Eu(L^5)_3][ClO_4]_3 \cdot 4MeCN$ **11** (see later), but the prisms are slowly transformed into thin needles when separated from the mother-liquor and elemental analyses of the isolated products are compatible with the formulations $[Ln(L^2)_3][ClO_4]_3 \cdot 0.5H_2O$ (Ln = Eu **6**, Gd **7** or Tb **8**) and $[Ln(L^5)_3][ClO_4]_3 \cdot 1.5H_2O$ (Ln = Eu **12**, Gd **13** or Tb **14**). The IR spectra show that the characteristic ligand vibrations at 1590 and 1520 cm^{-1} (C=C, C=N stretching) are slightly shifted toward high energy (1605, 1550 cm^{-1}) upon complexation to Ln^{III} in **6–8** and **12–14** as previously observed for $[Eu(L^1)_3][ClO_4]_3$ **5**.[10] The ClO_4^- anions all show the two expected symmetrical vibrations (1095, 625 cm^{-1}) typical of ionic perchlorate.[34]

We were unable to isolate 1:3 complexes with L^6 and only obtained very low yields (≈10%) of a 1:2 complex whose elemental analyses correspond to $[Eu(L^6)_2][ClO_4]_3 \cdot 5H_2O$ and which is insoluble in weakly co-ordinating solvents (acetonitrile, dichloromethane, *etc.*) and is decomplexed in co-ordinating solvents (methanol or water) giving L^6 and solvated Eu^{3+} as demonstrated by ^1H NMR measurements. Spectrophotometric titrations of L^6 with $Eu[ClO_4]_3$ show that no stable complexes are formed in acetonitrile at 10^{-4} mol dm^{-3} probably as a result of the steric interactions between the methyl groups bound to the 4 positions of the benzimidazole rings and the co-ordinated lanthanide ion. These complexes between L^6 and Ln^{III} were not further investigated.

Crystal Structure of $[Eu(L^5)_3][ClO_4]_3 \cdot 4MeCN$ **11**. Atomic coordinates are given in Table 2, selected bond lengths, angles and least-squares plane data in Table 3. Fig. 3 shows the atomic numbering scheme and Fig. 4 ORTEP[35] stereoscopic views

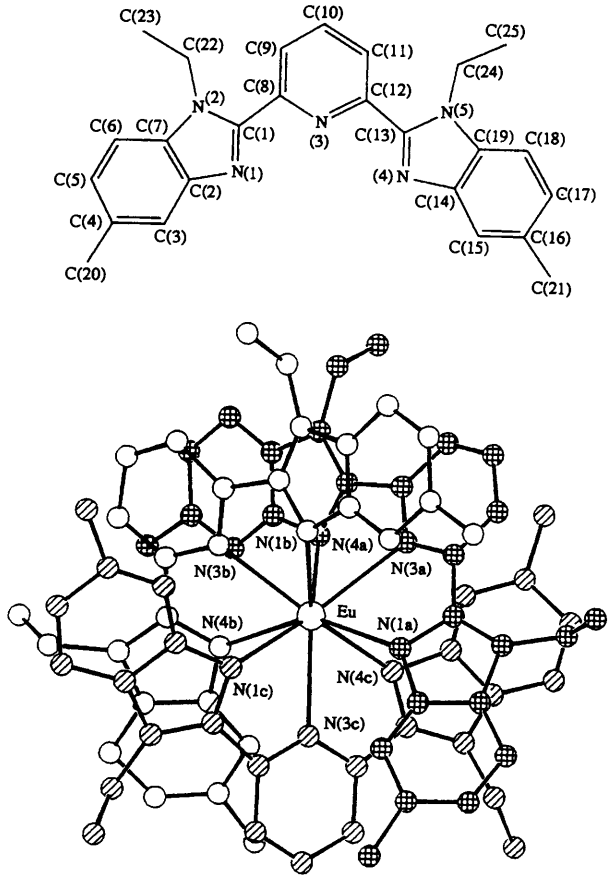

Fig. 3 Atomic numbering scheme for $[Eu(L^5)_3]^{3+}$

of the complex respectively perpendicular to and along the pseudo-C_3 axis.

In agreement with IR results, the crystal structure of compound **11** shows it to be composed of an $[Eu(L^5)_3]^{3+}$ cation, three unco-ordinated perchlorate anions and four acetonitrile molecules. The anions and solvent molecules are slightly disordered (see Experimental section) but otherwise show no features of interest. As previously reported for $[Eu(terpy)_3]^{3+}$,[12] $[Eu(L^1)_3]^{3+}$[10] and $[Eu(L^7)_3]^{3+}$,[14] the three ligands in $[Eu(L^5)_3]^{3+}$ are meridionally three-co-ordinated to the metal ion and wrapped about a pseudo-C_3 axis leading to a triple-helical structure. The co-ordination sphere around Eu^{III} may be best described as a slightly distorted trigonal tricapped prism where the six benzimidazole nitrogen atoms occupy the vertices of the prism and the three pyridine nitrogen atoms occupy the capping positions forming an equatorial plane (F3, Table 3) containing Eu^{III} [deviation from the F3 plane 0.030(4) Å]. The Eu–N bond distances (2.53–2.66 Å) do not significantly deviate from the average value [2.59(3) Å] found for $[Eu(L^1)_3]^{3+}$ [2.57–2.62 Å, average 2.59(1) Å][10] and $[Eu(L^7)_3]^{3+}$ [2.52–2.63 Å, average 2.58(2) Å][14] and calculation of the ionic radius of Eu^{III} using Shannon's definition[36] [r(N) = 1.46 Å] gives 1.13 Å for $[Eu(L^5)_3]^{3+}$ in agreement with the reported value for $[Eu(L^1)_3]^{3+}$ (1.13 Å).[10] The individual aromatic rings are planar within experimental error and the helical twisting of L^5 is achieved by twisting about the interannular C–C bonds between the pyridine and benzimidazole rings (Table 3). As described for $[Eu(L^1)_3]^{3+}$,[10] the helical wrapping of the ligands in $[Eu(L^5)_3]^{3+}$ leads to three possible intramolecular stacking interactions between almost parallel benzimidazole rings (bzb1–bza4, bzc1–bzb4, bza1–bzc4, Table 3), but a careful examination of the structure of $[Eu(L^5)_3]^{3+}$ shows that significant overlap between the benzimidazole rings only occurs

Table 2 Fractional atomic coordinates with estimated standard deviations (e.s.d.s) in parentheses for $[Eu(L^5)_3][ClO_4]_3 \cdot 4MeCN$ **11**

Atom	*X/a*	*Y/b*	*Z/c*	Atom	*X/a*	*Y/b*	*Z/c*
Eu	0.227 53(3)	0.110 79(2)	0.5	C(20b)	0.111 2(7)	0.144 5(6)	0.233(2)
N(1a)	0.195 1(6)	0.097 8(4)	0.370(1)	C(21b)	0.318 7(9)	0.020 8(6)	0.624(2)
N(2a)	0.195 8(5)	0.097 0(4)	0.229(1)	C(22b)	0.193 5(7)	0.210 8(5)	0.504(3)
N(3a)	0.237 2(4)	0.137 6(4)	0.369(1)	C(23b)	0.166 1(9)	0.224 7(6)	0.547(2)
N(4a)	0.277 2(4)	0.140 2(3)	0.500(2)	C(24b)	0.249 4(8)	0.103 4(6)	0.865(2)
N(5a)	0.281 9(4)	0.180 4(4)	0.494(2)	C(25b)	0.277 5(9)	0.114 6(8)	0.912(2)
C(1a)	0.203 8(7)	0.108 9(5)	0.297(2)	N(1c)	0.182 0(5)	0.094 2(4)	0.598(1)
C(2a)	0.178 3(7)	0.077 3(5)	0.344(2)	N(2c)	0.184 8(6)	0.069 7(5)	0.712(1)
C(3a)	0.164 2(7)	0.060 9(6)	0.392(2)	N(3c)	0.224 3(5)	0.064 8(3)	0.511(2)
C(4a)	0.150 5(8)	0.040 3(6)	0.358(2)	N(4c)	0.268 2(5)	0.086 1(4)	0.407(1)
C(5a)	0.150 8(8)	0.038 9(5)	0.271(3)	N(5c)	0.260 5(5)	0.057 7(4)	0.311(1)
C(6a)	0.164 2(9)	0.055 8(8)	0.220(2)	C(1c)	0.190 9(6)	0.072 9(5)	0.629(2)
C(7a)	0.179 0(7)	0.076 2(6)	0.258(2)	C(2c)	0.167 5(7)	0.105 1(6)	0.666(2)
C(8a)	0.220 9(6)	0.132 4(5)	0.298(1)	C(3c)	0.153 3(7)	0.127 9(6)	0.673(2)
C(9a)	0.220 3(8)	0.148 5(7)	0.234(2)	C(4c)	0.143 6(7)	0.136 6(6)	0.744(4)
C(10a)	0.235 2(8)	0.169 8(6)	0.241(2)	C(5c)	0.149(1)	0.122(1)	0.816(3)
C(11a)	0.252 8(8)	0.174 5(5)	0.310(2)	C(6c)	0.160(1)	0.099 2(9)	0.818(2)
C(12a)	0.252 6(6)	0.158 6(5)	0.376(1)	C(7c)	0.169 9(7)	0.091 1(5)	0.738(2)
C(13a)	0.269 7(7)	0.160 4(5)	0.456(2)	C(8c)	0.205 9(7)	0.055 0(5)	0.575(2)
C(14a)	0.296 6(7)	0.148 1(5)	0.568(2)	C(9c)	0.203 9(8)	0.029 2(5)	0.583(2)
C(15a)	0.314 1(6)	0.135 4(5)	0.631(2)	C(10c)	0.218 2(9)	0.015 9(5)	0.526(2)
C(16a)	0.330 1(7)	0.148 3(6)	0.691(2)	C(11c)	0.236 9(8)	0.025 9(5)	0.461(2)
C(17a)	0.329 8(8)	0.173 2(7)	0.690(2)	C(12c)	0.239 2(7)	0.051 4(5)	0.452(2)
C(18a)	0.314 7(8)	0.186 3(5)	0.627(2)	C(13c)	0.256 4(7)	0.065 2(5)	0.388(2)
C(19a)	0.298 9(7)	0.172 6(6)	0.567(2)	C(14c)	0.283 3(7)	0.092 7(6)	0.331(2)
C(20a)	0.134 1(8)	0.020 5(5)	0.406(2)	C(15c)	0.299 2(9)	0.112 9(7)	0.312(2)
C(21a)	0.347 8(6)	0.136 6(7)	0.759(3)	C(16c)	0.310 3(9)	0.117 9(7)	0.232(2)
C(22a)	0.204 0(8)	0.099 3(7)	0.141(2)	C(17c)	0.302(1)	0.100(1)	0.168(2)
C(23a)	0.173 7(9)	0.106 7(6)	0.091(2)	C(18c)	0.287(1)	0.079 1(8)	0.190(2)
C(24a)	0.281 3(8)	0.205 5(5)	0.465(2)	C(19c)	0.277 4(7)	0.074 9(6)	0.273(1)
C(25a)	0.313 1(8)	0.211 8(7)	0.419(2)	C(20c)	0.129 8(8)	0.160 5(5)	0.763(3)
N(1b)	0.183 5(4)	0.145 9(3)	0.484(1)	C(21c)	0.327(1)	0.142 0(8)	0.206(3)
N(2b)	0.186 8(5)	0.186 3(3)	0.487(2)	C(22c)	0.192 7(8)	0.049 2(5)	0.770(1)
N(3b)	0.224 2(5)	0.140 5(4)	0.620(1)	C(23c)	0.165 0(9)	0.032 9(6)	0.788(2)
N(4b)	0.258 5(6)	0.099 2(5)	0.638(2)	C(24c)	0.246 0(7)	0.036 5(5)	0.267(2)
N(5b)	0.257 6(6)	0.099 3(4)	0.774(1)	C(25c)	0.271 6(7)	0.015 8(4)	0.252(2)
C(1b)	0.194 2(6)	0.165 9(5)	0.523(2)	Cl(1)	0.227 4(3)	0.542 1(1)	0.496 3(8)
C(2b)	0.166 5(6)	0.155 2(5)	0.420(1)	O(1)	0.222(1)	0.531 8(6)	0.573(2)
C(3b)	0.146 9(5)	0.142 7(5)	0.360(1)	O(2)	0.231 9(9)	0.525 9(5)	0.432(2)
C(4b)	0.131 0(7)	0.157 2(7)	0.297(2)	O(3)	0.206 2(8)	0.561 6(5)	0.476(1)
C(5b)	0.137(1)	0.182 1(7)	0.296(2)	O(4)	0.257(1)	0.553 5(7)	0.502(4)
C(6b)	0.153 3(9)	0.194 4(6)	0.356(2)	Cl(2)	0.461 7(4)	0.579 5(3)	0.737(1)
C(7b)	0.167 9(6)	0.179 4(5)	0.419(2)	O(5)	0.445(1)	0.574 2(8)	0.813(3)
C(8b)	0.211 2(6)	0.163 0(5)	0.605(2)	O(6)*	0.442(2)	0.592(1)	0.686(5)
C(9b)	0.212 6(7)	0.181 9(4)	0.666(2)	O(7)*	0.483(2)	0.563(1)	0.698(4)
C(10b)	0.226 7(8)	0.176 5(5)	0.739(2)	O(8)*	0.478(2)	0.600(1)	0.773(5)
C(11b)	0.240 1(7)	0.152 4(5)	0.759(2)	O(81)*	0.494(3)	0.582(2)	0.718(7)
C(12b)	0.237 0(6)	0.135 9(5)	0.698(2)	Cl(3)	$\frac{1}{2}$	$\frac{1}{2}$	0.436(1)
C(13b)	0.249 4(6)	0.112 0(6)	0.704(2)	O(9)*	0.497(1)	0.519(1)	0.474(3)
C(14b)	0.274 0(7)	0.077 8(4)	0.661(2)	O(10)*	$\frac{1}{2}$	$\frac{1}{2}$	0.353(7)
C(15b)	0.289 7(6)	0.059 4(5)	0.616(2)	O(11)*	0.473(3)	0.508(2)	0.443(7)
C(16b)	0.301 6(7)	0.041 1(5)	0.665(2)	Cl(4)*	$\frac{1}{2}$	$\frac{1}{2}$	0.039(2)
C(17b)	0.300 1(7)	0.040 8(6)	0.749(3)	O(13)	0.514 7(7)	0.516 5(5)	0.002(3)
C(18b)	0.286 1(8)	0.059 4(6)	0.802(2)	O(14)*	0.494(6)	0.506(4)	0.094(7)
C(19b)	0.272 9(6)	0.078 4(4)	0.749(2)	O(15)*	0.471(2)	0.513(2)	0.082(6)

* Population 0.5.

for bzc1–bzb4 and bza1–bzc4 (contact distance 2.9–3.4 Å) while bzb1 and bza4 are almost parallel (1°; contact distance 3.08–3.22 Å), but shifted as a result of a significant anti-clockwise rotation of strand a and a clockwise rotation of strand b (Scheme 2, Figs. 3 and 4).

This distortion has been investigated quantitatively using a geometrical analysis of the co-ordination sphere around Eu^{III} in $[Eu(L^5)_3]^{3+}$, $[Eu(L^1)_3]^{3+}$ and $[Eu(L^7)_3]^{3+}$ based on the determination of the angles φ, θ_i and ω_i as depicted in Scheme 3. The pseudo-tricapped trigonal prisms around Eu^{III} are considered to be made up of three tripods: two are defined by the Eu–N(distal) vectors related by pseudo-C_3 symmetry [N(1a), N(1b), N(1c) and N(4a), N(4b), N(4c)] and one tripod is defined by the Eu–N(central) vectors [N(3a), N(3b), N(3c), Scheme 3]. In the first part of the analysis, the sum vectors R^1 = Eu–N(4a) + Eu–N(4b) + Eu–N(4c) and R^2 = Eu–N(1a) + Eu–N(1b) + Eu–N(1c) are calculated together with the angle φ between them which measures the average bending of the two distal tripods connected to the europium atom. The angles θ_i between R^1 and the Eu–N(4*i*) (*i* = a, b or c) vectors [or R^2 and Eu–N(1*i*) (*i* = a, b or c)] allow the quantitative determination of the flattening of the pseudo-trigonal prism along the pseudo-C_3 axis. Finally, we have calculated the projections of the nine nitrogen atoms {proj[N(*i*)]} onto a

Table 3 Selected bond distances (Å) and angles (°) and least-squares plane data for $[Eu(L^5)_3][ClO_4]_3 \cdot 4MeCN$ **11**

Eu–N(1a)	2.56(2)	Eu–N(3a)	2.60(2)	Eu–N(4a)	2.59(2)
Eu–N(1b)	2.66(2)	Eu–N(3b)	2.53(2)	Eu–N(4b)	2.61(2)
Eu–N(1c)	2.59(2)	Eu–N(3c)	2.56(2)	Eu–N(4c)	2.61(2)

N(1a)–Eu–N(3a)	65.5(7)	N(4a)–Eu–N(1c)	141.2(8)
N(1a)–Eu–N(4a)	125.3(8)	N(4a)–Eu–N(3c)	131.8(6)
N(1a)–Eu–N(1b)	77.5(6)	N(4a)–Eu–N(4c)	80.6(7)
N(1a)–Eu–N(3b)	140.3(7)	N(1b)–Eu–N(3b)	63.8(6)
N(1a)–Eu–N(4b)	149.2(8)	N(1b)–Eu–N(4b)	125.8(7)
N(1a)–Eu–N(1c)	91.2(7)	N(1b)–Eu–N(1c)	80.7(6)
N(1a)–Eu–N(3c)	75.5(8)	N(1b)–Eu–N(3c)	134.7(6)
N(1a)–Eu–N(4c)	73.7(7)	N(1b)–Eu–N(4c)	139.3(6)
N(3a)–Eu–N(4a)	61.6(7)	N(3b)–Eu–N(4b)	63.2(7)
N(3a)–Eu–N(1b)	66.8(6)	N(3b)–Eu–N(1c)	74.7(6)
N(3a)–Eu–N(3b)	104.3(7)	N(3b)–Eu–N(3c)	126.4(7)
N(3a)–Eu–N(4b)	138.3(7)	N(3b)–Eu–N(4c)	143.7(6)
N(3a)–Eu–N(1c)	142.8(6)	N(4b)–Eu–N(1c)	75.5(7)
N(3a)–Eu–N(3c)	129.2(8)	N(4b)–Eu–N(3c)	73.8(8)
N(3a)–Eu–N(4c)	75.3(6)	N(4b)–Eu–N(4c)	92.4(7)
N(4a)–Eu–N(1b)	93.5(6)	N(1c)–Eu–N(3c)	64.4(7)
N(4a)–Eu–N(3b)	68.4(7)	N(1c)–Eu–N(4c)	127.5(7)
N(4a)–Eu–N(4b)	77.3(8)	N(3c)–Eu–N(4c)	63.2(7)

Least-squares planes *		Deviation/Å	
		Max.	Atom
bza1	bzim, N(1a), N(2a)	0.04	C(3a)
pa3	py, N(3a)	0.03	C(11a)
bza4	bzim, N(4a), N(5a)	0.06	N(5a)
bzb1	bzim, N(1b), N(2b)	0.06	C(5b)
pb3	py, N(3b)	0.03	C(12b)
bzb4	bzim, N(4b), N(5b)	0.03	C(15b)
bzc1	bzim, N(1c), N(2c)	0.13	C(5c)
pc3	py, N(3c)	0.01	C(10c)
bzc4	bzim, N(4c), N(5c)	0.12	C(17c)
F1	N(1a), N(1b), N(1c)	—	—
F3	N(3a), N(3b), N(3c)	—	—
F4	N(4a), N(4b), N(4c)	—	—

Interplane angle (°)

	bza1	pa3	bza4	bzb1	pb3	bzb4	bzc1	pc3	bzc4	F1	F3
pa3	24										
bza4	43	23									
bzb1	44	23	1								
pb3	52	41	23	24							
bzb4	58	59	46	48	25						
bzc1	53	60	52	53	32	11					
pc3	42	62	68	69	58	43	32				
bzc4	13	37	53	53	56	56	49	31			
F1	34	43	43	44	32	25	19	26	31		
F3	27	38	41	42	35	32	26	27	24	7	
F4	20	34	42	43	40	40	34	28	17	15	8

* py = pyridine; bzim = benzimidazole. The rings are denoted as pyridine p or benzimidazole bz belonging to ligand strand a, b or c and possessing the nitrogen atom N(*i*). Thus bzc1 is the benzimidazole ring of strand c possessing the nitrogen atom N(1). The error in the dihedral angles between aromatic planes is typically 0.8°.

plane perpendicular to the R^1–R^2 direction and passing through Eu^{III}. The angles ω_i between the vectors Eu–proj[N(*i*)] belonging to the same ligand (intraligand, Table 4) show the deformation of the tricapped trigonal prism due to intraligand constraints while ω_i angles between Eu–proj[N(*i*)] belonging to different strands (interligand) show the deformation of the distal tripods from the trigonal prism toward the octahedron {*e.g.* ω_i between Eu–proj[N(1a)]–Eu–proj[N(4c)] is expected to be 60° for an octahedron and 0° for a trigonal prism} and the distortion of the capping positions. The values for φ, θ_i and ω_i are reported in Table 4 for each pseudo-tricapped trigonal prism. An identical geometrical analysis was performed with the normalized vectors $\langle Eu\text{–}N(i)\rangle = Eu\text{–}N(i)/\sqrt{[Eu\text{–}N(i)}$· Eu–N(*i*)] but the results are very close to those reported in Table 4 and were not considered further for the discussion.

For the three complexes $[Eu(L^5)_3]^{3+}$, $[Eu(L^1)_3]^{3+}$ and $[Eu(L^7)_3]^{3+}$, the φ angles (179–180°) do not significantly deviate from the expected value for a perfect trigonal prism (180°) indicating a small bending of the two distal tripods as confirmed by the almost parallel arrangement of the facial planes (F1, F3 and F4, Table 3) defined by the three nitrogen atoms of each tripod {0° for $[Eu(L^1)_3]^{3+}$, 7–8° for $[Eu(L^5)_3]^{3+}$}.

The average θ_i angles are very similar for the three complexes {$[Eu(L^5)_3]^{3+}$ (50), $[Eu(L^1)_3]^{3+}$ (52) and $[Eu(L^7)_3]^{3+}$ (50°)} suggesting a similar flattening of the trigonal prism along the pseudo-C_3 axis. For $[Eu(L^1)_3]^{3+}$ and $[Eu(L^7)_3]^{3+}$, the

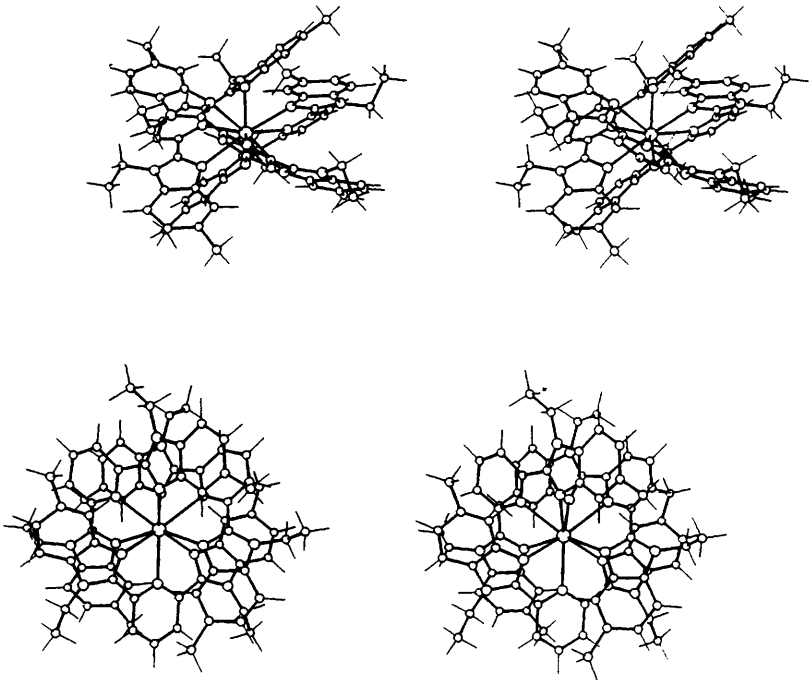

Fig. 4 ORTEP[35] stereoscopic views of $[Eu(L^5)_3]^{3+}$ perpendicular to the pseudo-C_3 axis and along it showing the intramolecular stacking interactions

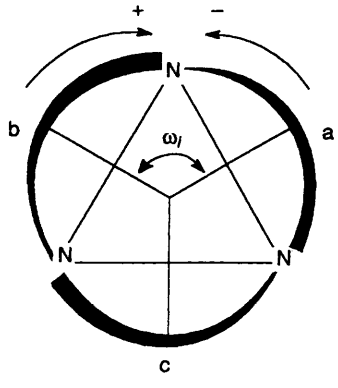

Scheme 2

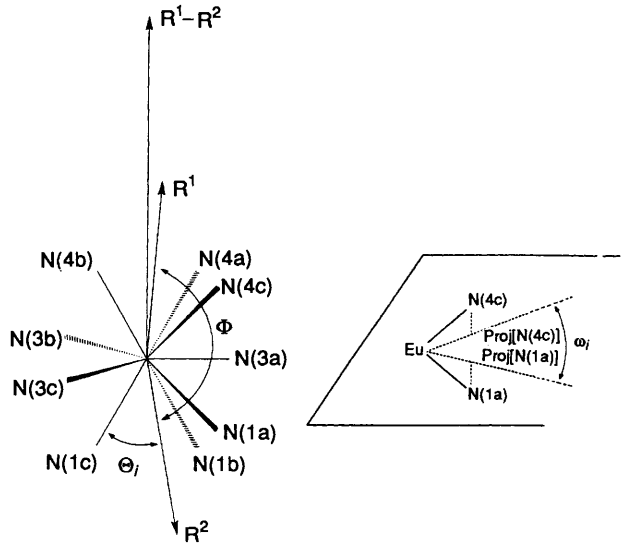

Scheme 3

individual θ_i angles do not greatly deviate from the average value indicating a rather regular arrangement of the two tripods. For $[Eu(L^5)_3]^{3+}$, the variation of the θ_i angles is more pronounced and R^2–Eu–N(1b) (θ_i = 44°) and R^1–Eu–N(4a) (θ_i = 44°) are significantly smaller than the average value as a result of the slide of strands a and b (Scheme 2) which shifts N(1b) to R^2 and N(4a) to R^1. This statement is exemplified by the ω_i angle between the Eu–proj[N(3a)] and Eu–proj[N(3b)] vectors which is only 104° for $[Eu(L^5)_3]^{3+}$ compared to 120° for a perfect tricapped trigonal prism {120° for $[Eu(L^1)_3]^{3+}$ and 113° for $[Eu(L^7)_3]^{3+}$} confirming the rotation of strands a and b in opposite directions about the pseudo-C_3 axis leading to a decrease of the N(3a)–Eu–N(3b) angle [104.3(7)°]. This deformation of the structure is probably responsible for the removal of the intramolecular stacking interactions between bzb1 and bza4 in $[Eu(L^5)_3]^{3+}$.

The intraligand ω_i angles in the three complexes are systematically smaller than 60°, the value expected for a perfect tricapped trigonal prism, which show that L^1, L^5 and L^7 slightly constrain the helical structure and induce a small distortion of the trigonal prism toward the octahedron if we only consider the two distal tripods. This is confirmed by the interligand ω_i angles of 10° {$[Eu(L^1)_3]^{3+}$}, 10–14° {$[Eu(L^5)_3]^{3+}$} and 11–12° {$[Eu(L^7)_3]^{3+}$} between the nitrogen atoms belonging to the distal tripods while the expected value for a perfect trigonal prism is 0 (60° for an octahedron).

The geometrical analysis shows that $[Eu(L^1)_3]^{3+}$ and $[Eu(L^7)_3]^{3+}$ possess slightly distorted pseudo-D_3 triple-helical structures while $[Eu(L^5)_3]^{3+}$ shows a more pronounced distortion from the perfect tricapped trigonal-prismatic arrangement. The origin of this effect is not obvious, but a careful examination of the structure of $[Eu(L^1)_3]^{3+}$ shows that the methyl groups bound to the benzimidazole rings are closely packed. More bulky R^3 groups (ethyl) in $[Eu(L^5)_3]^{3+}$ increase the steric constraints between the strands, as suggested by the opposite directions adopted by the ethyl groups in the crystal structure of compound **11** (Fig. 4), and results in a slide of the strands which shifts the R^3 groups leading to a decrease of the steric constraints and the removal of some stacking interactions. Contrary to the case of L^6 where the methyl groups bound to the benzimidazole rings prevent the complexation in solution, the methyl groups of L^5 are located close to the ends of the

Table 4 Structural data[a] for the europium co-ordination spheres in $[Eu(L^1)_3][ClO_4]_3$ **5**, $[Eu(L^5)_3][ClO_4]_3$ **11** and $[Eu(L^7)_3][ClO_4]_3$

	$[Eu(L^1)_3]^{3+}$	$[Eu(L^5)_3]^{3+}$	$[Eu(L^7)_3]^{3+}$
	Angles, φ/°		
R^1–Eu–R^2	180	179	180
	Angles, θ_i/° (distal tripods)		
R^1–Eu–N(1a)	51	52	48
R^1–Eu–N(1b)	51	44	51
R^1–Eu–N(1c)	51	54	52
R^1–Eu–N(4a)	52	44	52
R^1–Eu–N(4b)	52	52	47
R^1–Eu–N(4c)	52	54	52
	Angles, ω_i/° (intraligand)		
Proj[N(1a)]–Eu–Proj[N(3a)][b]	55	59	51
Proj[N(3a)]–Eu–Proj[N(4a)]	55	46	57
Proj[N(1b)]–Eu–Proj[N(3b)]	55	49	56
Proj[N(3b)]–Eu–Proj[N(4b)]	55	56	52
Proj[N(1c)]–Eu–Proj[N(3c)]	55	56	56
Proj[N(3c)]–Eu–Proj[N(4c)]	55	58	55
	Angles, ω_i/° (interligand)		
Proj[N(1a)]–Eu–Proj[N(4c)]	10	13	11
Proj[N(1b)]–Eu–Proj[N(4a)]	10	10	11
Proj[N(1c)]–Eu–Proj[N(4b)]	10	14	12
Proj[N(1a)]–Eu–Proj[N(3c)]	65	70	62
Proj[N(1a)]–Eu–Proj[N(3b)]	175	163	175
Proj[N(1b)]–Eu–Proj[N(3a)]	65	56	66
Proj[N(1b)]–Eu–Proj[N(3c)]	175	175	169
Proj[N(1c)]–Eu–Proj[N(3b)]	65	70	69
Proj[N(1c)]–Eu–Proj[N(3a)]	175	175	178
Proj[N(3a)]–Eu–Proj[N(3b)]	120	104	113
Proj[N(3b)]–Eu–Proj[N(3c)]	120	126	125
Proj[N(3a)]–Eu–Proj[N(3c)]	120	129	122

[a] For the definition of φ, θ_i and ω_i see text and Scheme 2. The error in the angles is typically 1°. [b] Proj[N(*i*)] is the projection of N(*i*) along the R^1–R^2 direction onto a perpendicular plane passing through the europium atom.

cylinder in $[Eu(L^5)_3]^{3+}$, but display no short contact distances with other atoms in the structure.

Examination of the crystal packing in compound **11** shows that the helical cations $[Eu(L^5)_3]^{3+}$ are arranged in layers parallel to the *ac* plane and separated by solvent molecules and perchlorate anions; the pseudo-C_3 axes of the complexes being roughly oriented along *a*.

Photophysical Properties of $[Ln(L^2)_3][ClO_4]_3$ (Ln = Eu **6**, Gd **7** *or* Tb **8**) *and* $[Ln(L^5)_3][ClO_4]_3$ (Ln = Eu **11** *and* **12**, Gd **13** *or* Tb **14**) *in the Solid State*.—The ligands L^1, L^2, L^5 and L^6 present, at 295 K and under excitation at 340 nm, two broad and structured emission bands (Fig. F1, SUP 57048). The first, between 350 and 450 nm, is assigned as arising from a $^1\pi\pi^*$ state. Its maximum is at 26 200 cm^{-1} for L^1, L^5, L^6 and at 26 800 cm^{-1} for L^2. One shoulder is observed on the low-energy side of the band at *ca.* 900–1100 cm^{-1} from the maximum. The second band has a sizable intensity for L^1 only; it is very weak for L^5 and weak for L^2 and L^6. It extends from 450 to 600 nm and arises from a $^3\pi\pi^*$ state as shown by the intensity increase when a pulsed excitation is used (308 nm) and by the long lifetimes (Table 5). In the Eu and Tb complexes with L^2 and L^5, the ligand luminescence is completely quenched, as observed previously for L^1.[10] It is also partly quenched in the Gd complexes **7** and **13** for which, however, the triplet-state luminescence is still observed, but with a much shorter lifetime.

The luminescence of the Eu complex **6** was analysed at 77 K in terms of the site symmetry of the metal ion.[5] The excitation spectrum presents an intense and large band centred at 400 nm and corresponding to excitation *via* the ligand singlet state, and several narrow and weak transitions corresponding to excitation through the metal ion levels, $^5L_6$, $^5D_2$, $^5D_1$ and $^5D_0$. The latter transition is comprised of two closely spaced components at 17 235 (site I) and 17 227 (site II) cm^{-1}, and of a shoulder at 17 220 cm^{-1} (Fig. F2, SUP 57048). Excitations through the ligand band and the $^5D_0 \longleftarrow {}^7F_0$ transitions yield the spectra reported in Fig. 5 and Table 6. The spectra resemble those reported for $[Eu(L^1)_3]^{3+}$,[10] with a predominance of the $^5D_0 \longrightarrow {}^7F_2$ and $^5D_0 \longrightarrow {}^7F_4$ transitions and an extremely weak $^5D_0 \longrightarrow {}^7F_0$ transition at 17 219 cm^{-1}. The corrected relative intensities amount to 0.0003, 1.0, 2.1, 0.1 and 1.5 for $J = 0$, 1, 2, 3 and 4, respectively. For site I, the local symmetry is very close to D_{3h}. For this point group the predicted number of components for the $^5D_0 \longrightarrow {}^7F_J$ transitions[5] is 0 for $J = 0$, 2 for $J = 1$ (magnetic dipole), 1 for $J = 2$ (electric dipole), 2 for $J = 3$ (magnetic dipole) and 3 for $J = 4$ (electric dipole). A close scrutiny of the emission spectrum reveals two additional, extremely weak components in the regions of the $^5D_0 \longrightarrow {}^7F_2$ and $^5D_0 \longrightarrow {}^7F_4$ transitions, that we assign to magnetic dipole processes. Site II displays a similar spectrum, with two slight differences with respect to the spectrum of site I: the E″ component of the $^5D_0 \longrightarrow {}^7F_1$ transition is split into two bands separated by 22 cm^{-1}, and so is one of the E′ components of the $^5D_0 \longrightarrow {}^7F_4$ transition (9 cm^{-1}). Its local symmetry can therefore be described as D_3 (number of allowed transitions in this symmetry: 0, 2, 2, 4 and 4 for $J = 0$, 1, 2, 3 and 4, respectively). It is noteworthy that laser excitation on the third

Table 5 Observed lifetimes (ms) at 77 K for ligands L^i (i = 1, 2, 5 or 6) and some of their Eu, Gd and Tb complexes measured at the analysis wavelength λ_{an}

Compound	λ_{exc}/nm	λ_{an}/nm	τ/ms
L^1	308, 370	450	190 ± 10*
L^2	308	525	160 ± 4
L^5	308	520	217 ± 10
L^6	308	535	195 ± 11
$[Gd(L^2)_3]^{3+}$ **7**	308	530	1.38 ± 0.03
$[Gd(L^5)_3]^{3+}$ **13**	308	540	0.94 ± 0.03
$[Eu(L^1)_3]^{3+}$ **5**	584.5	619.5	1.85 ± 0.04*
$[Eu(L^2)_3]^{3+}$ **6**	308	619	2.37 ± 0.05
	580.5	619	1.75 ± 0.05
$[Eu(L^5)_3]^{3+}$ **11**	581.1	616	1.75 ± 0.05
$[Eu(L^5)_3]^{3+}$ **12**	308	618.5	2.02 ± 0.02
	581.3	618.5	1.66 ± 0.07
$[Tb(L^1)_3]^{3+}$	488	544	1.46 ± 0.04*
$[Tb((L^2)_3]^{3+}$ **8**	488	544.2	1.95 ± 0.05
$[Tb(L^5)_3]^{3+}$ **14**	488	544.2	1.14 ± 0.04

* From ref. 10.

Table 6 Identified $Eu(^7F_J)$ energy levels (cm^{-1}, J = 1–4, origin $^7F_0$) in $[Eu(L^i)_3][ClO_4]_3$ complexes **6** and **11**, as calculated from luminescence spectra at 77 K[a]

	$[Eu(L^2)_3]^{3+}$		
Level	Site I	Site II	$[Eu(L^5)_3]^{3+}$
$^7F_1$	309	313	327
	416	400	364
		422	444
$^7F_2$	1010[b]	1009[b]	986
	1078 1086 (sh)	1075	1055
			1116
$^7F_3$	1821	1822	1840
$^7F_4$	2713	2701	2689
		2710	2723
	2758	2755	2787
	2868[b]	2863[b]	2868
	2983	2977	2976

[a] Excitation wavelengths: compound **6**, site I 580.23 nm, site II 580.48 nm; compound **11**, 580.76 nm. [b] Identified as a magnetic dipole transition.

component of the $^5D_0 \longleftarrow {}^7F_0$ transition, at 17 220 cm^{-1}, corresponding to the emission maxima of the ligand-excited luminescence spectrum, produces a spectrum identical with the spectrum of site II. We interpret the observation of two metal-ion sites in microcrystalline samples of compound **6** as arising from the presence of water in the crystal lattice (0.5 molecule per molecule of complex). In the case of a binuclear triple helical complex assembled from a dimer of L^4, L^8, we have indeed shown that the presence of water molecules in the lattice affects the crystal-field splittings of the J levels, but leaves the luminescence lifetime unchanged.[11] The lifetime of the $Eu(^5D_0)$ level, measured by direct laser excitation is long and similar for both sites, 1.60 for I and 1.75 ms for II. It does not reflect an inner-sphere interaction with water. When excitation is performed through the ligand band, the lifetime becomes longer, implying that the $^3\pi\pi^*$ state of the ligand is involved in the energy-transfer mechanism.

The $^5D_0 \longleftarrow {}^7F_0$ excitation spectrum at 77 K of single crystals of $[Eu(L^5)_3]^{3+}$ **11** presents one sharp band centred at 17 219 cm^{-1} (full width at half height 5 cm^{-1}), consistent with the presence of a single metal-ion environment. The emission spectrum (Fig. 6, Table 6) points to a substantial deviation from the idealized D_{3h} symmetry. The corrected relative intensities of the $^5D_0 \longrightarrow {}^7F_J$ transitions are 0.004, 1.0, 3.0, 0.2 and 2.2 for J = 0, 1, 2, 3 and 4 respectively. The number of observed main

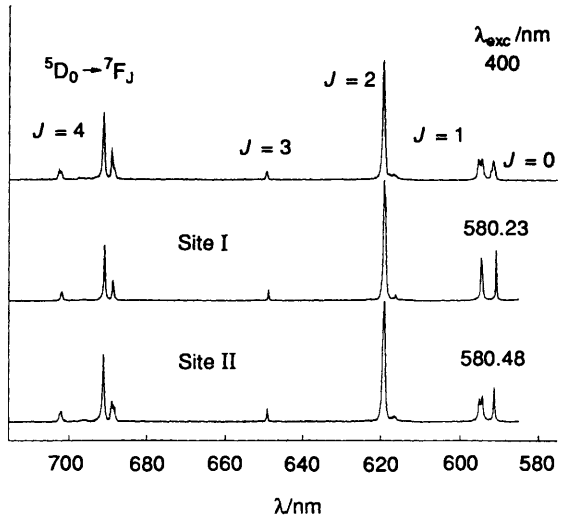

Fig. 5 Part of the emission spectra of $[Eu(L^2)_3][ClO_4]_3$ at 77 K under various excitation conditions. Vertical scale: arbitrary units

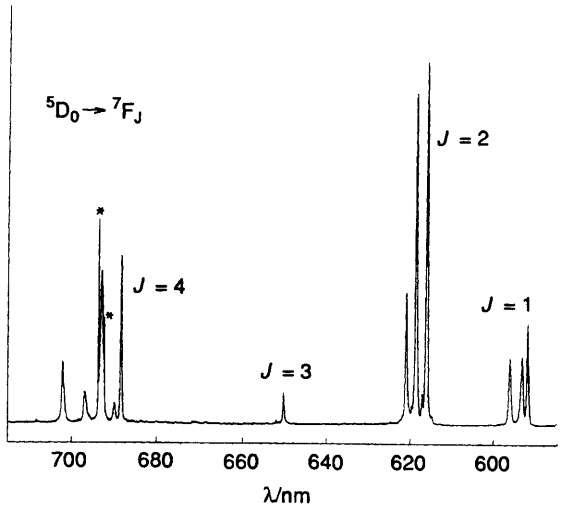

Fig. 6 Part of the laser-excited emission spectrum of single crystals of $[Eu(L^5)_3][ClO_4]_3$ **11** at 77 K (λ_{exc} = 580.76 nm). Vertical scale: arbitrary units. Asterisks denote emission bands from the argon plasma

components for the $^5D_0 \longleftarrow {}^7F_J$ transitions, 1, 3, 3 and 5 for J = 0, 1, 2 and 4, is consistent with a geometrical arrangement around the Eu^{III} ion having a C_{2v} or lower symmetry.[5] Microcrystalline samples of compound **12** display luminescence spectra the characteristics of which are close to those exhibited by the single crystals of **11**, at least as far as the intensities of the $^5D_0 \longrightarrow {}^7F_J$ transitions are concerned: 0.007, 1.0, 3.1, 0.1 and 1.8 for J = 0, 1, 2, 3 and 4 (Fig. F3, SUP 57048). As for compound **6**, however, the $^5D_0 \longleftarrow {}^7F_0$ excitation spectrum consists of several components, at 17 218, 17 227 and 17 231 cm^{-1}. Selective laser excitations of these bands yield spectra differing only partially and pointing to slightly different crystal-field effects in the various metal-ion environments. Again, we think that the presence of water in the lattice induces a different wrapping of the ligands around the metal ion, henceforth modifying the local symmetry. The lifetime of the $Eu(^5D_0)$ level is not affected by the presence of water in the lattice (Table 5) and increases when excitation is performed through the ligand band.

The luminescence spectra of the Tb complexes **8** and **14** are dominated by the $^5D_4 \longrightarrow {}^7F_5$ transition (Fig. F4, SUP 57048), as is usually the case for terbium complexes. The decays of the $Tb(^5D_4)$ luminescence are monoexponential. The lifetime for $[Tb(L^2)_3]^{3+}$ is somewhat longer than the lifetime of the

Table 7 Proton NMR chemical shifts (with respect to $SiMe_4$) for ligands L^i (i = 1–6) in $CDCl_3$ and complexes $[Ln(L^i)_3]^{3+}$ **5–14** in CD_3CN

Compound	H^1	H^2	H^3	H^4	H^5	H^6	$H^{7,8}$
L^1	7.85	7.20	—	7.40	8.42	8.05	4.25
L^2	7.85	7.30	—	7.40	8.36	8.06	4.81
L^3	7.85	7.30	—	7.40	8.33	8.04	4.71
L^4	7.82	7.22	—	7.38	8.39	8.02	5.54
L^5	7.66	—	7.20	7.37	8.30	8.04	4.78
L^6	—	7.15	7.20	7.40	8.34	8.05	4.74
$[Eu(L^1)_3]^{3+}$	13.43	7.53	7.29	5.67	2.80	4.85	1.81
$[Eu(L^2)_3]^{3+}$	11.73	7.20	7.28	5.70	3.60	5.77	2.07
							2.28
$[Eu(L^3)_3]^{3+}$	11.34	7.24	7.30	5.75	3.77	6.00	2.20
							2.50
$[Eu(L^4)_3]^{3+}$	11.32	7.37	7.29	5.74	3.52	5.68	3.50
							3.60
$[Eu(L^5)_3]^{3+}$	11.46	—	6.99	5.53	3.54	5.81	1.98
							2.14
$[Tb(L^1)_3]^{3+}$	−53.1	0.5	9.2	12.0	18.8	17.4	20.5
$[Tb(L^2)_3]^{3+}$	−44.5	3.5	12.0	13.9	16.2	17.4	7.4
							7.8
$[Tb(L^5)_3]^{3+}$	−44.8	—	11.9	13.8	16.4	17.8	7.4
							8.6

corresponding europium complex while $[Tb(L^5)_3]^{3+}$ has a much shorter lifetime (Table 5). This, combined with the fact that the complex with L^5 displays a far less intense luminescence than the compound with L^2, is indicative of a possible back transfer of energy to the ligand, as previously observed with similar compounds.[11] This observation suggests that the $\pi\pi^*$ excited states lie at lower energy for L^5 in agreement with absorption spectra and EHMO calculations.

Structure and Photophysical Properties of $[Ln(L^n)_3]^{3+}$ (n = 1–5) *in Solution*.—The ^1H NMR spectra of L^2 and L^5 display nine signals which were assigned through two-dimensional COSY and NOESY correlation spectroscopy (Table 7). Upon complexation to paramagnetic Eu^{III}, the signals of the protons are spread over 15 ppm as a result of contact and pseudo-contact shifts,[37] and we observe six aromatic signals for the complexes $[Eu(L^i)_3]^{3+}$ (i = 1–4) and five for $[Eu(L^5)_3]^{3+}$ together with diastereotopic AB spin systems for the methylene protons H^7, H^8 bound to the R^3 groups. These features have been already discussed in detail and correspond to D_3 symmetrical structures for the $[Eu(L^i)_3]^{3+}$ (i = 1–5) complexes on the NMR time-scale.[10] Examination of the chemical shifts of protons H^1–H^8 (Table 7) shows that $[Eu(L^i)_3]^{3+}$ (i = 2–5) display very similar spectra while that found for $[Eu(L^1)_3]^{3+}$ is significantly different as exemplified by H^1 which is shifted ≈2 ppm downfield. Since the connectivities and topologies are identical for $[Eu(L^i)_3]^{3+}$ (i = 1–5), we can reasonably assume comparable Fermi contact shifts[37] and the observed variations probably arise from different dipolar contributions strongly suggesting different arrangements of L^1 and L^i (i = 2–5) around Eu^{III}. These results indicate that the substitution of R^3 = H in L^1 by more bulky groups in L^i (i = 2–5) affects the wrapping of the ligands around the metal ion in solution as found in the crystal structures of $[Eu(L^1)_3]^{3+}$ [10] and $[Eu(L^5)_3]^{3+}$. The ^1H NMR spectra of $[Tb(L^i)_3]^{3+}$ (i = 1, 2 and 5), although more affected by paramagnetic effects,[37] confirm the D_3 symmetrical triple-helical structures on the NMR time-scale and the different behaviour of L^1 compared to L^2 and L^5.

As previously reported,[10] the size of R^3 affects the stability of the helical complexes in solution. For a 5×10^{-3} mol dm^{-3} solution in CD_3CN, only the 1:3 complexes $[Eu(L^i)_3]^{3+}$ (i = 1, 2 or 5) are observed in the ^1H NMR spectra while 10% of minor species arising from partial decomplexation of the aromatic rings[10,13] are observed for $[Eu(L^3)_3]^{3+}$ (R^3 = Et) and 30% for $[Eu(L^4)_3]^{3+}$ [R^3 = $C_6H_3(MeO)_2$-3,5]. Spectrophotometric titrations of L^2 and L^5 with $Eu(ClO_4)_3 \cdot 7H_2O$ in acetonitrile (Ln:ligand ratio in the range 0.1–1.8) show a complicated variation of the UV spectra as previously reported for L^i (i = 1, 3 or 4).[10] Factor analysis[38] implies the existence of four different absorbing species for each titration and the spectrophotometric data can be satisfactorily fitted with the successive formation of the three complexes $[Eu(L^i)_x]^{3+}$ (i = 1–5; x = 1–3). Unfortunately, the similarity of the calculated spectra for the three complexes (1:1, 1:2, 1:3)[10,11,39] prevents a precise determination of the stability constants (log β_i), but potentiometric studies based on competitions with H^+ and Ag^+ are currently in progress.

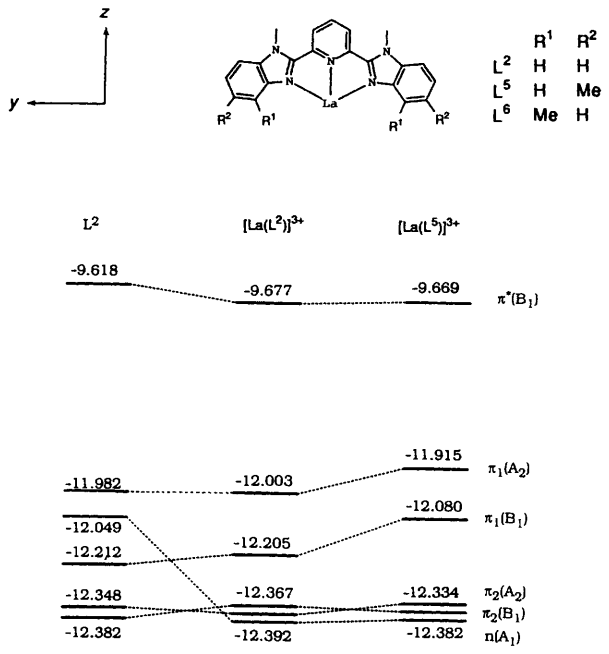

Fig. 7 Energy (in eV) of frontier orbitals calculated by EHMO[27] for L^2, $[La(L^2)]^{3+}$ and $[La(L^5)]^{3+}$ assuming C_{2v} symmetry

Upon complexation to Ln^{III}(Ln = Eu, Gd or Tb), the strong $\pi \longrightarrow \pi^*$ transitions centred on the ligand[18,25] are split into two main components (Table 1, Fig. 1) as previously described for 1:1 $[Ln(L^1)(NO_3)_3(MeOH)]$ (Ln = La, Nd, Eu, Gd or Tb),[20] 1:2 $[Lu(L^1)_2(H_2O)(MeOH)]^{3+}$,[10] 1:3 $[Ln(L^i)_3]^{3+}$ (i = 1, 3 or 4; Ln = La, Eu, Gd or Tb)[10] and for other complexes of L^1 with Cu^{II}, Zn^{II},[22] Cu^{I}[17] and Fe^{II}.[18] In an attempt to rationalize these observations we have performed EHMO calculations[27] for the $[La(L^i)]^{3+}$ fragment (i = 2 or 5) taking the structural parameters previously described for the ligands, but assuming that L^i (i = 2 or 5) are planar and symmetrically meridionally three-co-ordinated to La^{III} (cisoid conformations)[17,25] leading to C_{2v} symmetry (Fig. 7). Bond distances and angles for the co-ordination sphere around La^{III} were taken from the crystal structure of $[Eu(L^1)(NO_3)_3(MeOH)]$[20] with La–N(bzim) 2.7 and La–N(py) 2.6 Å.

The results show that the energy of the σ orbital centred on the pyridine ring [$n(A_1)$] is strongly affected by complexation as expected if we consider that EHMO usually overestimates the importance of covalent interactions,[27] particularly for Ln^{III} where these interactions are known to be weak.[40] Our simple EHMO approach is thus inadequate to give a quantitative description of the co-ordination bonds and we have limited our discussion to the general behaviour shown by the $\pi \longrightarrow \pi^*$ transitions in the UV spectra. Examination of Fig. 7 shows that the complexation of La^{3+} mainly stabilizes $\pi^*(B_1)$, but only slightly affects $\pi_1(A_2)$ and $\pi_1(B_1)$ leading to a shift of the $\pi_1 \longrightarrow \pi^*$ transitions toward lower energies. A similar effect is observed for the $\pi_2(B_1)$ and $\pi_2(A_2)$ and we expect the appearance

of $\pi_2 \longrightarrow \pi^*$ transitions on the high-energy side of the spectral window upon complexation of L^i to La^{III}. This is indeed qualitatively observed in the UV spectra of $[Eu(L^i)_3]^{3+}$ (i = 2 or 5, Fig. 1) and the previously reported 'splitting of $\pi \longrightarrow \pi^*$ upon complexation'[10,11,17,18,20,22] probably corresponds to a general shift of $\pi \longrightarrow \pi^*$ transitions toward lower energy leading to $\pi_1 \longrightarrow \pi^*$ around 27 000 cm^{-1} and $\pi_2 \longrightarrow \pi^*$ around 32 000 cm^{-1}. As previously observed for L^5, methyl groups bound to the 5 positions of the benzimidazole rings in $[Eu(L^5)_3]^{3+}$ shift the $\pi \longrightarrow \pi^*$ transitions to lower energies in good qualitative agreement with EHMO calculations which show a significant destabilization of $\pi_1(A_2)$ and $\pi_1(B_1)$ in $[La(L^5)]^{3+}$.

Luminescence Spectra of $[Eu(L^i)_3]^{3+}$ (i = 1–5) *in Solution.*—The emission spectra of the $[Eu(L^i)_3]^{3+}$ species in solution in anhydrous acetonitrile are extremely weak,[10,11] which prevented the determination of the $Eu(^5D_0)$ lifetimes. We have nevertheless succeeded in determining the quantum yields of these solutions relative to a solution of $[Eu(terpy)_3]^{3+}$ (Fig. 8, Table 8). Moreover, some unusual properties of these solutions were found upon dilution and upon addition of water or deuteriated water.

The measured quantum yields show all the $[Eu(L^i)_3]^{3+}$ solutions to be less luminescent than the $[Eu(terpy)_3]^{3+}$ solution by a factor of 10^3–10^4. The presence of low lying charge-transfer or ligand states may facilitate radiationless de-excitation through mixing with the Eu 4f states. Such a situation was found in a binuclear complex with *p-tert*-butylcalix[8]arene (4,11,18,25-tetra-*tert*-butyl[1.1.1.1]metacyclophane-7,14,21,28-tetrol), for which the ligand-to-metal charge-transfer state lies at only 20 000 cm^{-1}.[41] We have also shown that the relative quantum yields of solutions of europium mixed complexes with phenanthroline and substituted β-diketonates decrease by a factor 64 when the ligand absorption band is shifted from 30 300 to 25 600 cm^{-1}.[42] We were not able to locate the transition to the charge-transfer state for the $[Eu(L^i)_3]^{3+}$ species, because of probable overlap with the much more intense $\pi \longrightarrow \pi^*$ transitions. It is nevertheless certain that this charge-transfer state lies at higher energy than the state observed for the calix[8]arene complex. In comparison with $[Eu(terpy)_3]^{3+}$, the ligand $\pi \longrightarrow \pi^*$ transition for the $[Eu(L^i)_3]^{3+}$ species has an energy which is approximately 3300 cm^{-1} lower. This does not explain entirely the large difference in the quantum yields between $[Eu(L^i)_3]^{3+}$ and $[Eu(terpy)_3]^{3+}$ solutions. Solvent interaction may also contribute to non-radiative de-excitation but is not a predominant factor in our case: the complex with L^5, a ligand possessing methyl groups which should better protect the metal ion from external interaction, does not have the largest quantum yield. Finally, differences in decomplexation should not influence much the quantum yield data: the $[Ln(L^i)_3]^{3+}$ species have stability constants comparable to that of $[Ln(terpy)_3]^{3+}$ and the above-mentioned ^1H NMR experiments indicate that the triple-helical structure is maintained for $[Ln(L^i)_3]^{3+}$ (i = 1–5) and that substantial decomplexation (30% at 5 × 10^{-3} mol dm^{-3}) only occurs for $[Ln(L^4)_3]^{3+}$.

A surprising observation is that upon dilution of the $[Eu(L^i)_3]^{3+}$ solutions from 10^{-3} to 10^{-4} mol dm^{-3}, the total luminescence increases by a factor of 2–4, whereas the $[Eu(terpy)_3]^{3+}$ luminescence decreases linearly with the concentration. Concentration quenching is a commonly observed global phenomenon caused either by reabsorption of the emitted light by a neighbouring molecule or by de-excitation upon collision with another molecule to which part or the entirety of the energy is transferred. In our case, reabsorption can be ruled out since the ligand absorbs at much higher energy than the $^5D_0 \longrightarrow {}^7F_J$ transitions and direct reabsorption through the $^5D_0 \longleftarrow {}^7F_0$ transition is not probable in view of the extremely small absorption coefficient of this transition. Moreover, simple collisional de-excitation can also

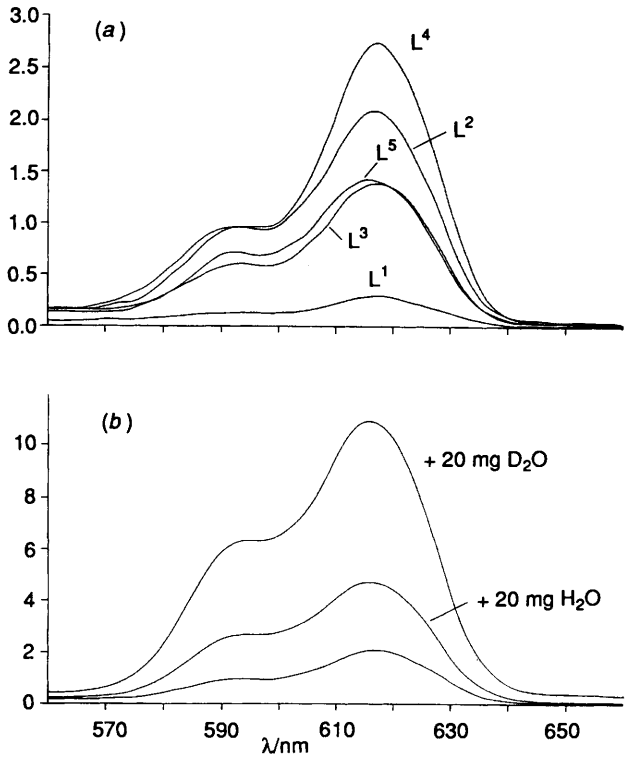

Fig. 8 Part of the luminescence spectra of $[Eu(L^i)_3]^{3+}$ solutions 10^{-3} mol dm^{-3} in anhydrous acetonitrile at 295 K (*a*) and modification of the spectrum for L^2 at 295 K upon addition of water and deuteriated water (*b*); excitation wavelengths: see Table 8. Vertical scales are given in arbitrary units

Table 8 Quantum yields at 296 K of $[Eu(L^i)_3]^{3+}$ solutions 10^{-3} mol dm^{-3} in anhydrous acetonitrile, relative to the quantum yield of a 10^{-3} mol dm^{-3} $[Eu(terpy)_3]^{3+}$ solution *

Compound	λ_{exc}/nm	η_{rel}	η_{rel}'
$[Eu(terpy)_3]^{3+}$	390	1.0	
$[Eu(L^1)_3]^{3+}$	414	6.3 × 10^{-5}	1.0
$[Eu(L^2)_3]^{3+}$	415	6.2 × 10^{-4}	9.8
$[Eu(L^3)_3]^{3+}$	419	4.8 × 10^{-4}	7.6
$[Eu(L^4)_3]^{3+}$	416	2.2 × 10^{-3}	35.0
$[Eu(L^5)_3]^{3+}$	427	5.9 × 10^{-4}	9.4

* Data are not corrected for possible decomplexation at this concentration; ^1H NMR spectra show this decomplexation to be small, except for L^4 (30%, see text).

be excluded since it does not occur in $[Eu(terpy)_3]^{3+}$ solutions. A possible explanation could be that decomplexation results in a less efficient intramolecular interaction between the ligand benzimidazole rings, thereby reducing the importance of the de-excitation processes. We have shown earlier that intramolecular electronic processes affect the luminescence intensity of macrocyclic complexes, for instance with calix[8]arene, in which interaction between the phenol units is partly responsible for a large luminescence quenching.[41] To investigate this hypothesis, we have added water and deuteriated water to the various solutions. Water molecules bind strongly to Ln^{3+} ions; they compete with the ligands and cause partial decomplexation. The latter has been shown by ^1H NMR spectroscopy for $[Eu(terpy)_3]^{3+}$.[12] Since O–H vibrators are very efficient quenchers of the Eu luminescence,[5] this results in a decrease of the emitted intensity for the $[Eu(terpy)_3]^{3+}$ solution. On the other hand, the addition of 10 equivalents of water to the $[Eu(L^i)_3]^{3+}$ solutions leads to a substantial increase in the luminescence intensity, except for $[Eu(L^5)_3]^{3+}$,

for which the intensity decreases slightly. Further addition of water confirms this trend, and addition of deuteriated water causes the same effect, but to a larger extent. Even for $[Eu(L^5)_3]^{3+}$ the luminescence is enhanced by addition of D_2O. This luminescence enhancement is expected if the partial decomplexation of the ligand causes less interaction between the benzimidazole rings. The additional luminescence enhancement generated by the addition of deuteriated water is consistent with the water molecules entering in the inner co-ordination sphere of the europium ion, since O–D oscillators are known to be poor quenchers of the $Eu(^5D_0)$ luminescence.

Finally, the data reported in Table 8 reflect the influence of the R^3 substituents on the quantum yields. When the alkyl chain is lengthened, the quantum yield increases by almost an order of magnitude. It is noteworthy that the introduction of an additional methyl group in R^2 does not affect the quantum yield, despite the better protection against external interaction of the lanthanide ion along the pseudo-C_3 axis. The most dramatic luminescence enhancement occurs when bulky 3,5-dimethoxybenzyl substituents are introduced in R^3. This again supports the hypothesis made for explaining the luminescence variation of the $[Eu(L^5)_3]^{3+}$ solutions since a bulky R^3 substituent will cause steric hindrance and further diminish the interaction between the ligand strands.

Conclusion

The synthesis of the ligands L^i (i = 1–6) offers the possibility to investigate some of the factors controlling the structure and the photophysical properties of the triple-helical building blocks $[Ln(L^i)_3]^{3+}$. Except for L^6 where steric constraints prevent complexation, all the ligands L^i (i = 1–5) react with Ln^{III} to give mononuclear pseudo-D_3 triple-helical complexes in solution and in the solid state. Crystal structure, photophysical studies and ^1H NMR measurements of $[Ln(L^i)_3]^{3+}$ (i = 1–5) show that the size of R^3 controls the structure of the triple helix and its stability, but the binding of methyl groups to the 5 positions of the benzimidazole rings mainly affects the electronic properties by shifting $^1\pi\pi^*$ toward lower energies. The most striking feature of the complexes $[Eu(L^i)_3]^{3+}$ (i = 1–5) concerns their low quantum yields in acetonitrile which are surprisingly increased when water is added to the solution. Although the relative importance of the various quenching processes in $[Eu(L^i)_3]^{3+}$ is not completely elucidated, we have established that an important factor leading to the low quantum yields is associated with the triple-helical structures resulting from the wrapping of three ligands around the metal ion: this ligand arrangement is favourable to intramolecular interactions between the benzimidazole moieties, leading to efficient radiationless processes. Further attempts to increase the luminescence of these building blocks should deal with specific modifications of the distal co-ordinating groups in order to change the vibrational and electronic properties, and the intramolecular stacking interactions. Our simple EHMO approach seems to be promising in this context since electronic effects may be qualitatively predicted by using a simple model.

Experimental

Solvents and Starting Materials.—These were purchased from Fluka AG (Buchs, Switzerland) and used without further purification, unless otherwise stated. Dimethylformamide was distilled from CaH_2, dichloromethane and chloroform (analytical grade) were filtered over basic aluminium oxide (Merck activity I) prior to use. All reactions were carried out under nitrogen if not stated otherwise. Aluminium oxide (Merck activity II–III, 0.063–0.200 mm) and Silicagel (Merck 60, 0.040–0.060 mm) were used for preparative column chromatography.

Preparation of the Ligands.—2,6-Bis(1′-X-benzimidazol-2′-yl)pyridine [X = Me L^1, Pr L^3, or $CH_2C_6H_3(OMe)_2$-3,5 L^4] were prepared according to a published two-step procedure.[10,17,22] 2,6-Bis(1′-ethylbenzimidazol-2′-yl)pyridine (L^2) was obtained according to the same method but using ethyl iodide as the alkylating agent. The crude product was purified by column chromatography (Silicagel, CH_2Cl_2–MeOH 99.3:0.7 to 98:2) then crystallized from dichloromethane–hexane (yield 91%). M.p. 185–186 °C, δ_H(300 MHz, $CDCl_3$) 1.38 [6 H, t, J(HH) 7, CH_2CH_3], 4.81 [4 H, q, J(HH) 7, CH_2CH_3], 7.30–7.45 (4 H, m), 7.50 (2 H, m), 7.85–7.90 (2 H, m), 8.06 [1 H, t, J(HH) 8], 8.36 [2 H, d, J(HH) 8 Hz]; m/z 367 (M^+), 352 ($M - CH_3$), 338 ($M - CH_2CH_3$).

Synthesis of 4-(N-*Ethylamino*)-3-*nitrotoluene* **1**.—4-Chloro-3-nitrotoluene (5 g, 29 mmol) and ethylamine (60 cm^3, 70% in water) were heated at 130 °C for 24 h in an autoclave. The mixture was evaporated to dryness and the resulting red oil shaken with concentrated hydrochloric acid (35 cm^3). The organic layer was separated, extracted with concentrated hydrochloric acid (2 × 15 cm^3) and the combined aqueous phases were neutralized (pH 9) with aqueous 5 mol dm^{-3} NaOH. The resulting solution was extracted with dichloromethane (2 × 150 cm^3) and the combined organic phases evaporated to dryness and crystallized from hot hexane to give **1** (3.48 g, 67%) as orange crystals. M.p. 52–53 °C. TLC (Silicagel, CH_2Cl_2) R_f = 0.58; δ_H(300 MHz, $CDCl_3$) 1.37 [3 H, t, J(HH) 7, CH_2CH_3], 2.27 (3 H, s), 3.34 [2 H, dq, J(HH) 7, 5, CH_2CH_3], 6.77 [1 H, d, J(HH) 8], 7.27 [1 H, dd, J(HH) 8, 2], 7.88 (1 H, br s), 7.98 [1 H, d, J(HH) 2 Hz]; m/z 180 (M^+), 165 ($M - CH_3$), 119 ($M - CH_3 - NO_2$).

Synthesis of 3-(N-*Ethylamino*)-2-*nitrotoluene* **2**.—3-Amino-2-nitrotoluene (1 g, 6.57 mmol), Na[BH_3(CN)] (1.48 g, 23.6 mmol) and acetic acid (8 cm^3) were dissolved in methanol (100 cm^3). Acetaldehyde (0.318 g, 7.23 mmol) in methanol (40 cm^3) was added dropwise for 8 h, and then the mixture was stirred for 15 h at room temperature. Concentrated hydrochloric acid (8 cm^3) in water (80 cm^3) was added and methanol evaporated under vacuum. The aqueous phase was neutralized with saturated aqueous $NaHCO_3$, extracted with dichloromethane (3 × 100 cm^3), dried over Na_2SO_4 and evaporated to dryness. The crude product was purified by column chromatography (Silicagel; hexane–CH_2Cl_2 92.5:7.5) then distilled (90 °C at 0.01 Torr, *ca.* 1.33 Pa) to give **2** (0.774 g, 65%) as a red oil. TLC (Silicagel, CH_2Cl_2) R_f = 0.60; δ_H(300 MHz, $CDCl_3$) 1.29 [3 H, t, J(HH) 7, CH_2CH_3], 2.45 (3 H, s), 3.22 [2 H, dq, J(HH) 7, 5, CH_2CH_3], 6.40 (1 H, br s), 6.49 [1 H, d, J(HH) 8], 6.63 [1 H, d, J(HH) 8], 7.19 [1 H, t, J(HH) 8 Hz]; m/z 180 (M^+), 165 ($M - CH_3$), 119 ($M - CH_3 - NO_2$).

Synthesis of Bis[N-*ethyl*-N-(4′-*methyl*-2′-*nitrophenyl*)]-*pyridine*-2,6-*dicarboxamide* **3**.—Compound **1** (0.59 g, 3.25 mmol) and triethylamine (1.65 g, 16.3 mmol) were refluxed in dry dichloromethane (50 cm^3) and solid 2,6-di(chlorocarbonyl)pyridine (0.5 g, 2.45 mmol) was added in small portions for 12 h. The resulting mixture was refluxed for 15 h, evaporated to dryness, partitioned between dichloromethane (150 cm^3) and half-saturated aqueous NH_4Cl (150 cm^3). The organic layer was separated, evaporated to dryness and the crude product purified by column chromatography (Silicagel, CH_2Cl_2–MeOH 99.75:0.25 ⟶ 99.5:0.5) to give **3** (0.527 g, 66%) as a pale yellow powder. M.p. 55 °C (decomp.). TLC (Silicagel, CH_2Cl_2–MeOH 95:5) R_f = 0.46; $\tilde{\nu}/cm^{-1}$ 3080w (aromatic CH), 2980m (saturated CH), 2940m, 2880w, 1660s (CO); δ_H(300 MHz, $CDCl_3$) 0.8–1.3 [6 H, m, CH_2CH_3], 2.18–2.50 [6 H, m, aryl CH_3], 3.4–4.5 (4 H, m, CH_2CH_3), 6.9–8.0 (9 H, m, aromatic); m/z 492 (M^+), 446 ($M - NO_2$).

The same procedure was followed for the synthesis of bis-[*N*-ethyl-*N*-(3′-methyl-2′-nitrophenyl)]pyridine-2,6-dicarboxamide **4** in 64% yield from **2**. M.p. 160–161 °C; TLC (Silicagel, CH_2Cl_2–MeOH 95:5) R_f = 0.50; $\tilde{\nu}/cm^{-1}$ 3090w

Table 9 Elemental analyses for complexes **6–8** and **12–14**

Complex	Analysis (%)* C	H	N
6	53.15 (53.05)	4.15 (4.15)	13.40 (13.45)
7	52.95 (52.90)	4.15 (4.10)	13.35 (13.40)
8	53.00 (52.85)	4.05 (4.10)	13.40 (13.40)
12	54.10 (54.15)	4.75 (4.75)	12.60 (12.65)
13	54.05 (53.95)	4.70 (4.70)	12.60 (12.60)
14	54.05 (53.90)	4.75 (4.70)	12.60 (12.55)

* Calculated values in parentheses.

(aromatic CH), 2980m (saturated CH), 2940m, 2880w, 1660vs (CO); δ_H(300 MHz, $CDCl_3$) 1.0–1.4 (6 H, m, CH_2CH_3), 2.2–2.4 (6 H, m, aryl CH_3), 3.2–4.4 (4 H, m, CH_2CH_3), 6.8–7.8 (9 H, m, aromatic); *m/z* 492 (M^+), 446 ($M - NO_2$).

Synthesis of 2,6-*Bis*(1'-*ethyl*-5'-*methylbenzimidazol*-2'-*yl*)*pyridine* (L^5).—Compound **3** (0.488 g, 0.993 mmol) was dissolved in ethanol–water (4:1, 350 cm^3). Activated iron powder (1.68 g, 30 mmol) and concentrated hydrochloric acid (37%, 6.2 cm^3, 74 mmol) were added and the mixture refluxed for 20 h. Water (30 cm^3) was then added, excess of iron filtered off and ethanol distilled under vacuum. The resulting mixture was poured into CH_2Cl_2 (100 cm^3), $Na_2(H_2edta)\cdot 2H_2O$ (H_4edta = *N*,*N*,*N*',*N*'-ethylenediaminetetraacetic acid) (4.5 g) dissolved in water (40 cm^3) was added and the resulting stirred mixture neutralized (pH 8.5) with 12% aqueous NH_4OH. Concentrated hydrogen peroxide (30%, 2 cm^3) was added under vigorous stirring. After 15 min, the organic layer was separated and the aqueous phase extracted with CH_2Cl_2 (2 × 100 cm^3). The combined organic phases were dried over Na_2SO_4, evaporated to dryness and the crude residue purified by column chromatography (Silicagel, CH_2Cl_2–MeOH 99.3:0.7 to 95:5) then crystallized from dichloromethane–hexane to give L^5 (0.329 g, 91%) as white crystals. M.p. 213–214 °C; TLC (Silicagel, CH_2Cl_2) R_f = 0.35; δ_H(300 MHz, $CDCl_3$) 1.36 [6 H, t, *J*(HH) 7, CH_2CH_3], 2.54 (6 H, s), 4.78 [4 H, q, *J*(HH) 7, CH_2CH_3], 7.20 [2 H, dd, *J*(HH) 8, 1.3], 7.35 [2 H, d, *J*(HH) 8], 7.66 (2 H, br s), 8.04 [1 H, t, *J*(HH) 8], 8.30 [2 H, d, *J*(HH) 8 Hz]; *m/z* 395 (M^+), 380 ($M - CH_3$), 366 ($M - CH_2CH_3$).

The same procedure was followed for the synthesis of 2,6-bis(1'-ethyl-4'-methylbenzimidazol-2'-yl)pyridine (L^6) from **4** in 93% yield. M.p. 143–144 °C; TLC (Silicagel, CH_2Cl_2) R_f = 0.34; δ_H(300 MHz, $CDCl_3$) 1.34 [6 H, t, *J*(HH) 7, CH_2CH_3], 2.77 (6 H, s), 4.74 [4 H, q, *J*(HH) 7, CH_2CH_3], 7.15 [2 H, d, *J*(HH) 8], 7.23–7.35 (4 H, m), 8.05 [1 H, t, *J*(HH) 8], 8.34 [2 H, d, *J*(HH) 8 Hz]; *m/z* 395 (M^+), 380 ($M - CH_3$), 366 ($M - CH_2CH_3$).

Preparation of Lanthanide Complexes.—The perchlorate salts $Ln(ClO_4)_3\cdot nH_2O$ (Ln = Eu, Gd or Tb; *n* = 6–8) were prepared from the corresponding oxide (Glucydur, 99.99%) according to a literature method.[43] The complexes $[Eu(L^1)_3][ClO_4]_3\cdot H_2O$ **5**, $[Eu(L^3)_3][ClO_4]_3\cdot H_2O$ **9** and $[Eu(L^4)_3][ClO_4]_3\cdot 5H_2O$ **10** were prepared according to published procedures.[10]

Preparation of $[Ln(L^2)_3][ClO_4]_3\cdot 0.5H_2O$ (Ln = Eu **6**, Gd **7** *or* Tb **8**) *and* $[Ln(L^5)_3][ClO_4]_3\cdot 1.5H_2O$ (Ln = Eu **12**, Gd **13** *or* Tb **14**).—Compounds $Ln(ClO_4)_3\cdot nH_2O$ (*n* = 6–8) (0.126 mmol) in acetonitrile (2 cm^3) were slowly added to a solution of L^2 or L^5 (0.042 mmol) in dichloromethane–acetonitrile (1:1, 5 cm^3). The resulting solution was evaporated to dryness, the solid residue dissolved in acetonitrile and diethyl ether slowly diffused into the solution for 3 d to give white (Ln = Gd or Tb) or yellow (Ln = Eu) X-ray quality prisms of $[Ln(L^2)_3][ClO_4]_3\cdot 0.5H_2O$ **6–8** and $[Ln(L^5)_3][ClO_4]_3\cdot 1.5H_2O$ **12–14** in 72–83% yield. All these complexes **6–8** and **12–14** were characterized by their IR spectra and gave satisfactory elemental analyses (Table 9).

CAUTION: Perchlorate salts with organic ligands are potentially explosive and should be handled with the necessary precautions.[44]

Crystal-structure Determination of $[Eu(L^5)_3][ClO_4]_3\cdot$ 4MeCN **11**.—Crystals were prepared as previously described and sealed with mother-liquor in capillaries.

Crystal data. $C_{83}H_{87}Cl_3EuN_{19}O_{12}$, *M* = 1801.0, orthorhombic, space group *Fdd*2, *a* = 40.641(6), *b* = 55.515(8), *c* = 15.979(4) Å, *U* = 36052(7) Å^3 [by least-squares refinement of 28 reflections (15 ⩽ 2θ ⩽ 25°)], *Z* = 16, D_c = 1.33 g cm^{-3}, *F*(000) = 14 848. Yellow prisms. Crystal dimensions 0.35 × 0.35 × 0.50 mm for the {100}, {010} and {001} faces respectively, μ(Mo-Kα) = 0.847 mm^{-1}.

Data collection and processing. Stoe STADI4 diffractometer, ω–2θ mode with ω scan width = 1.05 + 0.35 tan θ, ω scan speed 0.06–0.12° s^{-1}, graphite monochromated Mo-Kα radiation; 10 396 reflections measured (6 ⩽ 2θ ⩽ 42°, 0 < *h* < 40, 0 < *k* < 56, 0 < *l* < 16), 9705 unique reflections (R_{int} for equivalent reflections = 0.055) of which 7429 were observable [$|F_o| > 4\sigma(F_o)$]. Two reference reflections were measured every 45 min and showed a variation in intensity < 3.7σ(*I*).

Structure analysis and refinement. Data were corrected for Lorentz and polarization and for absorption effects[45] (A^*_{min} = 1.281, A^*_{max} = 1.313). The structure was solved by direct methods using MULTAN 87;[46] all other calculations used the XTAL[47] system and ORTEP II[35] programs. Atomic scattering factors and anomalous dispersion terms were taken from ref. 48. Refinements (on *F*) were performed with four blocked matrices (ligand a and europium, ligand b, ligand c, perchlorates and solvent molecules; maximum number of variables = 966). The europium, nitrogen and carbon atoms of the ligands and the chlorine atoms were refined with anisotropic displacement parameters (98 atoms) and all the other atoms (23) with isotropic displacement parameters. Two perchlorate anions are found in general positions (one is slightly disordered and refined with five atomic positions for the oxygen atoms) and two in special positions 8a (C_2 axis). Both perchlorates are disordered and refined with six atomic positions for the oxygen atoms (site occupancy factors: see Table 2). From the four solvent molecules, three were observed with three atomic sites and one with two atomic sites. Final *R* factors *R* = *R*' = 0.062 (*w* = 1) for 966 variables and 7429 contributing reflections. As a result of the disorder observed for the perchlorates and solvent molecules, a weighting scheme with *w* = 1 was used to avoid unreasonable anisotropic displacement parameters which are obtained with the usual statistical scheme. The mean shift/error on the last cycle was 0.041 and the maximum 1.17. Hydrogen atoms were placed in calculated positions and contributed to F_c calculations. The final Fourier difference synthesis showed a maximum of +0.86 and a minimum of −1.46 e Å^{-3}. The chirality/polarity of the structure was refined and the absolute structure parameter[49] converged to *x* = 0.20(3). The polar origin was fixed by constraining the *z* coordinate of the Eu atom at 0.5.

Additional material available from the Cambridge Crystallographic Data Centre comprises H-atom coordinates, thermal parameters and remaining bond lengths and angles.

Spectroscopic and Analytical Measurements.—Electronic spectra in the UV/VIS range were recorded at 20 °C from 10^{-3} mol dm^{-3} acetonitrile solutions with a Perkin-Elmer Lambda 5 spectrometer using quartz cells of 0.01 cm path length. Spectrophotometric titrations were performed with a Perkin-Elmer Lambda 5 spectrophotometer connected to an external computer. In a typical experiment, 50 cm^3 of ligand (L) in

acetonitrile (10^{-4} mol dm^{-3}) were titrated with a 2.5 × 10^{-3} mol dm^{-3} solution of $Eu(ClO_4)_3 \cdot 7H_2O$ in acetonitrile. After each addition of 0.20 cm^3, the absorbances at 10 different wavelengths were recorded using a 0.1 cm quartz cell and transferred to the computer. Plots of absorbance as a function of the metal–ligand ratio gave a first indication of the number and stoichiometry of the complexes formed: factor analysis[38] was then applied to the data to confirm the number of different absorbing species. Finally, a model for the distribution of the species was fitted with a non-linear least-squares algorithm to give stability constants as previously described.[50] The IR spectra were obtained from KBr pellets with a Perkin-Elmer 883 spectrometer. Proton and ^{13}C NMR spectra were recorded on a Varian Gemini 300 spectrometer. Chemical shifts are given in ppm with $SiMe_4$ as reference. Electron ionization mass spectra (70 eV) were recorded with VG 7000E and Finnigan 4000 instruments. Luminescence measurements were performed on a previously described instrumental set-up.[20,51] Solid-state samples were finely powdered, except for some of the Eu and Tb crystals with no hydration water which were measured in acetonitrile–diethyl ether. Luminescence spectra are corrected for the instrumental function, but not excitation spectra. Lifetimes are averages of at least three independent determinations. Relative luminescence quantum yields were determined using a Perkin-Elmer LS-50 spectrofluorimeter. Anhydrous acetonitrile was obtained as previously described.[52] The solutions were prepared under a nitrogen atmosphere in a glove-box and were thoroughly degassed with argon. The spectra were measured in phosphorescence mode (delay time 0.01 ms, gate time 1.0 ms, cycle time 200 ms) and each spectrum was the result of five accumulations (excitation bandpath 15 nm, analysing bandpath 20 nm). Water or deuteriated water was directly injected into the solutions using a Hamilton micropipette. The relative quantum yields were calculated using equation (1),[7] where subscript r stands for the reference and x

$$Q_x/Q_r = \langle A_r(\lambda_r)/A_x(\lambda_x)\rangle\langle I(\lambda_r)/I(\lambda_x)\rangle\langle n^2{}_x/n^2{}_r\rangle\langle D_x/D_r\rangle \quad (1)$$

for the samples; A is the absorbance at the excitation wavelength, I is the intensity of the excitation light at the same wavelength, n is the refractive index (1.341 for all the solutions) and D is the integrated luminescence intensity. Cyclic voltammograms were recorded using a Cypress System potentiostat connected to a personal computer. A three-electrode system consisting of a stationary Pt disk working electrode, a Pt counter electrode, and a non-aqueous $Ag–Ag^+$ reference electrode was used. NBu_4PF_6 (0.1 mol dm^{-3} in MeCN) served as inert electrolyte and MeCN was distilled from P_2O_5 and then passed through an Alox column (activity I). The reference potential ($E° = -0.11$ V *vs.* SCE) was standardized against $[Ru(bipy)_3][ClO_4]_2$ (bipy = 2,2′-bipyridyl).[53] The scan speed used was 100 mV s^{-1} and voltammograms were analysed according to established procedures.[53] Extended Hückel calculations[27] were performed with program ICON8 using the standard parameters for the carbon, nitrogen and hydrogen atoms,[27] and tested empirical parameters for the lanthanum (Table SII, SUP 57048).[54] Elemental analyses were performed by Dr. H. Eder of the Microchemical Laboratory of the University of Geneva.

Acknowledgements

We gratefully thank Ms. Véronique Foiret and Mr. Bernard Bocquet for their technical assistance. J.-C. B. thanks the Fondation Herbette (Lausanne) for the gift of spectroscopic equipment. This work is supported through grants from the Swiss National Science Foundation.

References

1 J. F. Tangay and S. L. Suib, *Catal. Rev. Sci. Eng.*, 1987, **29**, 1.
2 M. J. P. Leiner, *Anal. Chim. Acta*, 1991, **255**, 209.
3 V.-M. Mukkala, M. Helenius, I. Hemmilä, J. Kankare and H. Takalo, *Helv. Chim. Acta*, 1993, **76**, 1361.
4 F. S. Richardson, *Chem. Rev.*, 1982, **82**, 541; A. K. Saha, K. Kross, E. D. Kloszewski, D. A. Upson, J. L. Toner, R. A. Snow, C. D. V. Black and V. C. Desai, *J. Am. Chem. Soc.*, 1993, **115**, 11032.
5 J.-C. G. Bünzli, in *Lanthanide Probes in Life, Chemical and Earth Sciences*, eds. G. R. Choppin and J.-C. G. Bünzli, Elsevier, Amsterdam, 1989, ch. 7, p. 219.
6 V. Balzani, N. Sabbatini and F. Scandola, *Chem. Rev.*, 1986, **86**, 319; J.-M. Lehn, in *Frontiers in Supramolecular Organic Chemistry and Photochemistry*, eds. H.-J. Schneider and H. Dürr, VCH, Weinheim, 1991, p. 1; N. Sabbatini, M. Guardigli and J.-M. Lehn, *Coord. Chem. Rev.*, 1993, **123**, 201.
7 J.-M. Lehn and J.-B. Regnouf de Vains, *Helv. Chim. Acta*, 1992, **75**, 1221; V. M. Mukkala and J. J. Kankare, *Helv. Chim. Acta*, 1992, **75**, 1578; V. M. Mukkala, C. Sund, M. Kwiatotkowski, P. Pasanen, M. Högberg, J. J. Kankare and H. Takalo, *Helv. Chim. Acta*, 1992, **75**, 1621; M. Pietraszkiewicz, S. Pappalardo, P. Finocchiano, A. Mamo and J. Karpiuk, *J. Chem. Soc., Chem. Commun.*, 1990, 1907; V. Balzani, J.-M. Lehn, J. Van Loosdrecht, A. Mecati, N. Sabbatini and R. Ziessel, *Angew. Chem., Int. Ed. Engl.*, 1991, **30**, 190.
8 B. Alpha, J.-M. Lehn and G. Mathis, *Angew. Chem., Int. Ed. Engl.*, 1987, **26**, 266; B. Alpha, V. Balzani, J.-M. Lehn, S. Perathoner and N. Sabbatini, *Angew. Chem., Int. Ed. Engl.*, 1987, **26**, 1266; J.-M. Lehn, M. Pietraszkiewicz and J. Karpiuk, *Helv. Chim. Acta*, 1990, **73**, 106; N. Sabbatini, A. Mecati, M. Guardigli, V. Balzani, J.-M. Lehn, R. Ziessel and R. Ungaro, *J. Lumin.*, 1991, **48–49**, 463.
9 V. Balzani, E. Berghmans, J.-M. Lehn, N. Sabbatini, A. Mecati, R. Therorde and R. Ziessel, *Helv. Chim. Acta*, 1990, **73**, 2083; L. Prodi, M. Maestri, R. Ziessel and V. Balzani, *Inorg. Chem.*, 1991, **30**, 3798; R. Ziessel, M. Maestri, L. Prodi, V. Balzani and A. van Doersselaer, *Inorg. Chem.*, 1993, **32**, 1237.
10 C. Piguet, J.-C. G. Bünzli, G. Bernardinelli and A. F. Williams, *Inorg. Chem.*, 1993, **32**, 4139.
11 C. Piguet, J.-C. G. Bünzli, G. Bernardinelli, G. Hopfgartner and A. F. Williams, *J. Am. Chem. Soc.*, 1993, **115**, 8197.
12 G. H. Frost, F. A. Hart and M. B. Hursthouse, *Chem. Commun.*, 1969, 1421; D. A. Durham, G. H. Frost and F. A. Hart, *J. Inorg. Nucl. Chem.*, 1969, **31**, 833.
13 R. D. Chapman, R. T. Loda, R. W. Riehl and R. W. Schwartz, *Inorg. Chem.*, 1984, **23**, 1652.
14 C. Mallet, R. P. Thummel and C. Hery, *Inorg. Chim. Acta*, 1993, **210**, 223.
15 R. P. Thummel and Y. Jahng, *J. Org. Chem.*, 1985, **50**, 2407; V. Hedge, Y. Jahng and R. P. Thummel, *Tetrahedron Lett.*, 1987, **28**, 4023; C.-Y. Huang, L. A. Cabell and E. V. Anslyn, *J. Am. Chem. Soc.*, 1994, **116**, 2778.
16 J. D. Crane and J.-P. Sauvage, *New. J. Chem.*, 1992, **16**, 649; J. P. Sauvage and M. D. Ward, *Inorg. Chem.*, 1991, **30**, 3869.
17 C. Piguet, G. Bernardinelli and A. F. Williams, *Inorg. Chem.*, 1989, **28**, 2920; S. Rüttimann, C. Piguet, G. Bernardinelli, B. Bocquet and A. F. Williams, *J. Am. Chem. Soc.*, 1992, **114**, 4230.
18 C. G. Bochet, C. Piguet and A. F. Williams, *Helv. Chim. Acta*, 1993, **76**, 372.
19 C. Piguet, G. Hopfgartner and B. Bocquet, *Helv. Chim. Acta*, 1994, **77**, 931.
20 C. Piguet, A. F. Williams, G. Bernardinelli, E. Moret and J.-C. G. Bünzli, *Helv. Chim. Acta*, 1992, **75**, 1697.
21 S. Wang, Q. Luo, X. Zhou and Z. Zeng, *Polyhedron*, 1993, **12**, 1939.
22 C. Piguet, B. Bocquet, E. Müller and A. F. Williams, *Helv. Chim. Acta*, 1989, **72**, 323.
23 R. F. Borch, M. D. Bernstein and H. D. Durst, *J. Am. Chem. Soc.*, 1971, **93**, 2897; P. H. Morgan and A. H. Beckett, *Tetrahedron*, 1975, **31**, 2595.
24 W. Oppolzer, P. Cintas-Moreno, O. Tamura and F. Cardinaux, *Helv. Chim. Acta*, 1993, **76**, 187.
25 K. Nakamoto, *J. Phys. Chem.*, 1960, **64**, 1420; E. C. Constable, S. M. Elder, J. V. Walker, P. P. Wood and D. A. Tocher, *J. Chem. Soc., Chem. Commun.*, 1992, 229.
26 D. W. Fink and W. E. Ohnesorge, *J. Phys. Chem.*, 1970, **74**, 72.
27 R. Hoffmann, *J. Chem. Phys.*, 1963, **39**, 1397; R. Hoffmann and W. N. Lipscomb, *J. Chem. Phys.*, 1962, **37**, 2872, 3179, 3489.
28 R. M. Berger and D. R. McMillin, *Inorg. Chim. Acta*, 1990, **177**, 65.
29 T. L. Gilchrist, *Heterocyclic Chemistry*, Longman, Harlow, 1987, p. 13; J. March, *Advanced Organic Chemistry*, 3rd edn., Wiley, Chichester, 1985, p. 19.
30 D. R. Kearns and M. A. El-Bayouni, *J. Chem. Phys.*, 1963, **38**, 1508.
31 I. Fleming, *Frontier Orbitals and Organic Chemical Reactions*, Wiley, Chichester, 1976, p. 80.

32 J. M. Rao, M. C. Hughes and D. J. Macero, *Inorg. Chim. Acta*, 1976, **16**, 231; 1980, **41**, 221.
33 J. E. Figard and J. D. Petersen, *Inorg. Chem.*, 1978, **17**, 1059; C. Malouf and P. C. Ford, *J. Am. Chem. Soc.*, 1977, **99**, 7213.
34 K. Nakamoto, *Infrared and Raman Spectra of Inorganic and Coordination Compounds*, 3rd edn., Wiley, New York, 1972, p. 142.
35 C. K. Johnson, ORTEP II, Report ORNL-5138, Oak Ridge National Laboratory, Oak Ridge, Tennessee, 1976.
36 R. D. Shannon, *Acta Crystallogr., Sect. A*, 1976, **32**, 751.
37 I. Bertini and C. Luchinat, *NMR of Paramagnetic Molecules in Biological Systems*, Benjamin and Cummings, Menlo Park, CA, 1986, ch. 10.
38 E. R. Malinowski and D. G. Howery, *Factor Analysis in Chemistry*, Wiley, New York, 1980.
39 F. R. Hartley, C. Burgess and R. M. Alcock, *Solution Equilibria*, Ellis Horwood, Chichester, 1980.
40 R. Reisfeld and C. K. Jørgensen, *Lasers and Excited States of Rare Earths, in Inorganic Chemistry Concepts*, Springer Verlag, Berlin, 1977, vol. 1, ch. 3; G. R. Choppin, in *Lanthanide Probes in Life, Chemical and Earth Sciences*, eds. G. R. Choppin and J.-C. G. Bünzli, Elsevier, Amsterdam, 1989, ch. 1, p. 18.
41 J.-C. G. Bünzli, P. Froidevaux and J. M. Harrowfield, *Inorg. Chem.*, 1993, **32**, 3306; P. Froidevaux and J.-C. G. Bünzli, *J. Phys. Chem.*, 1994, **98**, 532.
42 J.-C. G. Bünzli, E. Moret, V. Foiret, K. J. Schenk, W. Mingzhao and J. Linpei, *J. Alloys & Compounds*, in the press.
43 J. F. Desreux, in *Lanthanide Probes in Life, Chemical and Earth Sciences*, eds. G. R. Choppin and J.-C. G. Bünzli, Elsevier, Amsterdam, 1989, ch. 2, p. 43.
44 W. C. Wolsey, *J. Chem. Educ.*, 1973, **55**, A355.
45 E. Blanc, D. Schwarzenbach and H. D. Flack, *J. Appl. Crystallogr.*, 1991, **24**, 1035.
46 P. Main, S. J. Fiske, S. E. Hull, L. Lessinger, D. Germain, J. P. Declercq and M. M. Woolfson, MULTAN 87, Universities of York and Louvaine-La-Neuve, 1987.
47 *XTAL 3.2 User's Manual*, eds. S. R. Hall and J. M. Stewart, Universities of Western Australia and Maryland, 1989.
48 *International Tables for X-Ray Crystallography*, Kynoch Press, Birmingham, 1974, vol. 4.
49 G. Bernardinelli and H. D. Flack, *Acta Crytallogr., Sect. A*, 1985, **41**, 500.
50 C. Piguet, G. Bernardinelli, B. Bocquet, A. Quattropani and A. F. Williams, *J. Am. Chem. Soc.*, 1992, **114**, 7440.
51 P. Guerriero, P. A. Vigato, J.-C. G. Bünzli and E. Moret, *J. Chem. Soc., Dalton Trans.*, 1990, 647; P. Froidevaux, Ph.D. Thesis, Université de Lausanne, 1992.
52 J.-C. G. Bünzli, J.-P. Metabanzoulou, P. Froidevaux and J. Linpei, *Inorg. Chem.*, 1990, **29**, 3875.
53 A. J. Bard and L. R. Faulkner, *Electrochemical Methods, Fundamentals and Application*, Wiley, New York, 1980.
54 L. A. Bengtsson and R. Hoffmann, *J. Am. Chem. Soc.*, 1993, **115**, 2666.

Received 19*th July* 1994; *Paper* 4/04414B